Impact of Ocean Acidification on Recruitment and Yield of Bristol Bay Red King Crab

Dušanka Poljak

A thesis
submitted in partial fulfillment of the
requirements for the degree of

Master of Science

University of Washington
2013

Committee:
André E. Punt
Michael G. Dalton
Ray W. Hilborn

Program Authorized to Offer Degree:
School of Aquatic and Fishery Sciences

In presenting this thesis in partial fulfillment of the requirements for a Master's degree at the University of Washington, I agree that the Library shall make its copies freely available for inspection. I further agree that extensive copying of this thesis is allowable for scholarly purposes consistent with "fair use" as prescribed by the U.S. Copyright Law. Any other reproduction for any other purposes or by any means shall not be allowed without my written permission.

Signature_____

Date_____

University of Washington

Abstract

Impact of Ocean Acidification on Recruitment and Yield of Bristol Bay Red King Crab

Dušanka Poljak

Chair of the Supervisory Committee:
Professor André E. Punt
School of Aquatic and Fishery Sciences

The excess of anthropogenic carbon dioxide (CO_2) produced since the industrial revolution is being absorbed by the oceans through the carbon cycle. Atmospheric carbon dioxide has increased about 40% since the preindustrial era, and the oceans have absorbed more than a third of these emissions. This has led to the release of H^+ ions via seawater carbonate chemistry, and hence to a reduction in ocean pH, that is, ocean acidification. Ocean pH has been reduced by roughly 0.1 units, which is equivalent to an increase in H^+ of roughly 30%, and about a 16% decrease in CO_3^{-2}. Corrosive waters, the waters below the $CaCO_3$ saturation horizon, are predicted to reach shallower depths more in the Northeast Pacific Ocean than in any other ocean basin. The saturation horizon is projected to reach the surface of the North Pacific Ocean during this century, and some regions of the Bering Sea are predicted to become carbon shell corrosive seasonally by the middle of this century, which will expose a wide range of North Pacific species, including Bristol Bay Red king crab, to corrosive waters.

Bristol Bay Red king crab has been one of the most valuable fished stocks in the US. It is managed by the State of Alaska under federal guidelines defined in the Fishery Management Plan (FMP) for crab in the Bering Sea and Aleutian Islands. Current management rules are designed to handle short-term fluctuations in stock abundance

mainly due to exploitation. The impact of ocean acidification on red king crab is predicted to lead to long-term changes to stock abundance, and for which management is currently unprepared.

This thesis explores the impact of ocean acidification on recruitment and yield of Bristol Bay red king crab under a range of ocean acidification scenarios and management strategies. The management strategies include setting the exploitation rate for the directed fishery to that under the overfishing limit (OFL) rule, applying constant exploitation rates, and setting exploitation rates that maximize catch and discounted profit. Trends in recruitment to the first size-class in the stock assessment model are estimated using a pre-recruit model in which survival is parameterized based on experimental results from the NMFS Kodiak laboratory. Exploitation rates are estimated, and time series (2000-2100) for MMB, catch, and discounted profit are projected, for each management strategy for three levels of variable fishery costs and for the economic discount factor.

The catch, biomass, and discounted profit equilibrate at non-zero values for the no-OA scenario, but are driven to zero for all exploitation rates in the OA scenarios. Lower constant exploitation rates lead to a longer time before the biomass is driven close to zero, but the total discounted profit is highest at the highest exploitation rate for the three OA scenarios. The OFL control rule performs better than the constant exploitation rate strategies in terms of conserving the resource, because this rule closes the fishery at low biomass levels, which are also unprofitable. Estimated total discounted profits for the strategies which maximize catch and discounted profit are about the same for the base no-OA scenario, while the strategy that maximizes profit leads to slightly higher discounted profit and it depletes the stock below the biomass threshold sooner than the strategy which maximizes catch. Catches are the same for the strategies which maximize catch for no-OA scenario, and are higher for the strategy which maximizes catch for the OA scenarios. Higher discount rates lead to higher biomasses and catches, and the fishery is closed earlier for higher costs (food, fuel, and bait costs) for the OA scenarios when exploitation rates are selected to maximize profit.

TABLE OF CONTENTS

LIST OF TABLES

LIST OF FIGURES

ACKNOWLEDGEMENTS

I want to thank Michael Dalton, my supervisor at AFSC from three years ago. Mike gave me the opportunity to further my education and career in collaboration with André Punt, my adviser today and chair committee. This degree would not have happened without Mike's initial support and André's willingness to work with me. I am deeply appreciative of their efforts and continued support.

To my adviser and committee chair, André Punt, thank you for all your time, will, and patience in sharing your expertise. Also thank you for the many, many revisions. The support you provided was boundless in every way. You helped me to grow beyond what I thought I could do. I could not have asked for more. It has been my pleasure and honor to work with you. I am inspired by your hard work, dedication, integrity, and kindness regardless the hour.

A special thanks to my committee members: Dr. Michael Dalton, Dr. André Punt, and Dr. Ray Hilborn. Thank you for your valuable contributions and expert insight, and thank you for permitting me as many discussions and suggestions as I requested. I have leaned a lot more than I expected coming into the program, and I am happy for it. It has been my pleasure.

Thank you to my lab-mates Chantell Wetzel, Cody Szuwalski, Felipe Hurtado Ferro, Ingrid Spies, Pamela Woods, and Kelli Johnson for always being present and in a good grad student mood, always curious, ready to work, help, have fun, or ponder over any question with great attention and curiosity that might arise. It would not have been the same without you.

Lastly, a heartfelt thanks to my mom in Croatia for living this journey with me, and to my American family of friends for always being there for me making all good things better.

Chapter 1: Ocean Acidification

1.1. Ocean Acidification

The pH level of the oceans is regulated through the carbon cycle in which carbon circulates among the atmosphere, the land, and the oceans, in response to the chemical imbalance of carbon concentrations among the systems. The carbon cycle is an equilibrium reaction, and the imbalances in carbon concentrations or carbon partial pressures among the three systems creates a carbon flux, where the environment with the lowest amount of carbon, currently the oceans, acts as a sink. The strength of the carbon intake depends on the strength of the flux. The greater the difference in carbon partial pressures, the stronger the flux, and the more carbon is absorbed by the oceans (Raven et al., 2005).

Atmospheric carbon dioxide (CO_2) has increased about 40% since the preindustrial era, i.e., from ~280 ppm (parts per million) to ~384 ppm in 2007 (IPCC, 2007). CO_2 is predicted to exceed ~600 ppm by 2100, with a possibility to reach ~1000 ppm (Caldeira et al., 2003). The growth rate of CO_2 averaged 1.4 ppm per year over 1960-2005, with an average of 1.9 ppm per year over the ten-year period 1995-2005. The change in CO_2 is attributed to anthropogenic activities, mainly fuel combustion and deforestation (Doney and Schimel, 2007). The surface of the ocean, defined as the water layer to approximately 100m in depth, plays a critical role in CO_2 absorption. Over the past 200 years, the oceans have absorbed more than a third of the CO_2 emissions:

$$\text{Air-sea exchange: } CO_{2(atmos)} \rightleftharpoons CO_{2(aq)} \tag{1.1}$$

This has altered the seawater carbonate chemistry and hence the ocean pH by roughly 0.1 units of pH, which is equivalent to an increase in H^+ of roughly 30%, and approximately a 16% decrease in CO_3^{-2} (Feely et al., 2004; Fabry et al., 2008). The CO_2 absorbed by the ocean will remain in the surface layer for several years before it is transported to depth via vertical mixing. Vertical mixing of ocean water (sinking and upwelling) to depths of 1000 - 4000m can take several hundred years or more, which causes the surface waters to be slightly less alkaline than the deep waters. This phenomenon is caused by horizontal layering of different pH levels in the ocean. Consequently, most of the CO_2 derived from human activities has yet to reach the deep oceans.

After CO_2 is absorbed by the ocean (Equation 1.1), it reacts with water (H_2O) to form a weak carbonic acid (H_2CO_3):

$$CO_{2(aq)} + H_2O \rightleftharpoons H_2CO_3 \rightleftharpoons H^+ + HCO_3^- \rightleftharpoons 2H^+ + CO_3^{2-} \tag{1.2}$$

H_2CO_3 dissociates to a hydrogen ion (H^+) and a bicarbonate ion (HCO_3^-). The resulting H^+ reacts with carbonate ions (CO_3^{2-}) to produce HCO_3^- ions. As a result, CO_2 dissolution in the ocean leads to an increase in H^+ (thus a decrease in pH) and a decrease in CO_3^{2-} concentration. Carbon cycle reactions (Equations 1.1 and 1.2) are used to predict future change to the world's ocean pH level under specified IPCC IS92a CO_2 scenarios (IPCC, 2001). It is projected that the ocean pH level will decline by 0.14-0.35 pH units by the year 2100 (IPCC, 2001).

Dissolved CO_2 in seawater exists in three main inorganic forms known as dissolved inorganic carbon (DIC): (i) aqueous CO_2 (approximately 1% of the total), (ii) bicarbonate (HCO_3^-, approximately 91%), and (iii) carbonate ions (CO_3^{2-},approximately 8%). All three forms play important roles in the biological processes of marine organisms, including photosynthesis (production of food and energy from sunlight) done mainly by phytoplankton, and calcification (building structures such as $CaCO_3$ shells) mainly done by crustaceans. The part of the dissolved CO_2 which does not facilitate biological processes sinks to the bottom of the ocean as sediment.

1.2. The saturation horizon

The $CaCO_3$ saturation state (Ω) is the product of the concentrations of Ca^{2+} and CO_3^{2-} divided by the apparent stoichiometric solubility product K_{sp}^* for both types of $CaCO_3$ (aragonite or calcite) commonly secreted by marine organisms:

$$\Omega = [Ca^{+2}][CO_3^{2-}] / K_{sp}^* \tag{1.3}$$

Calcium concentration Ca^{+2} is estimated from salinity, and CO_3^{2-} concentration is calculated from DIC and total alkalinity measurements. Increasing levels of marine CO_2 decrease levels of CO_3^{-2} (Equation 1.2) thereby lowing $CaCO_3$ saturation levels. Regions with $\Omega > 1$ are above the saturation horizon and favor formation of shells and skeletons, whereas regions with $\Omega < 1$ are below the saturation horizon and are corrosive to $CaCO_3$, and dissolution is likely to occur (Fabry et al., 2008).

Oceanic water is not homogeneously saturated by minerals. Some parts of the ocean are supersaturated and others undersaturated in terms of carbonate ions. The transition between supersaturated and undersaturated conditions is referred to as the saturation horizon (see Equation 1.3). The levels of saturation in the ocean differ among depths and geographic locations. Shallow and warm oceanic waters tend to be supersaturated with respect to calcite and aragonite, whereas deep and cold-temperature waters tend to be undersaturated. Hence, deep and cold waters are more likely to dissolve calcium carbonate shells (Secretariat of the Convention on Biological Diversity, 2009).

In addition to the saturation level, several other physical factors impact dissolution of $CaCO_3$. Factors that increase dissolution of $CaCO_3$ usually occur in deeper water, such as higher pressures, lower temperatures, and lower pH (Sigler et al., 2008). Independent of depth, incorporation of other minerals such as magnesium, into carbonate ions also increases their solubility. Corrosive waters, the waters below the $CaCO_3$ saturation horizon, are predicted to reach shallower depths more in the Northeast Pacific Ocean than in any other ocean basin. The $CaCO_3$ saturation horizon is shallower in the North Pacific Ocean (~200m) compared to that in the North Atlantic Ocean (~2,000m) (Feely et al., 2004; Sigler et al., 2008). The saturation horizon is projected to reach the surface of the North Pacific Ocean during this century (Orr et al., 2005; Sigler et al., 2008), which will expose a wide range of North Pacific species to corrosive waters (Sigler et al., 2008). Consequently, ocean acidification will have a greater impact on marine organisms in the northeast Pacific Ocean, compared to other regions (NOAA Ocean Acidification Steering Committee, 2010).

1.3. The role of $CaCO_3$ in calcifying organisms

Calcifying organisms, such as most mollusks, corals, crustaceans, echinoderms, foraminifera and calcareous algae use carbon to grow shells. Among species there is variation in chemical structures and processes that govern calcification, but the principal steps are similar in each case. Many calcifying organisms investigated demonstrate reduced calcification in response to increased CO_2 concentration, decreased concentration of CO_3^{2-}, decreased $CaCO_3$ saturation state, and lower pH (e.g. Gattuso et al., 1998; Langdon et al., 2000; Riebesell et al., 2000). Among the multicellular organisms, the crustaceans may be the most vulnerable group because of their dependence on the availability of calcium and bicarbonate ions during the multiple molting stages that take place during their lives (Raven et al., 2005; Sigler et al., 2008).

To make calcareous shells, sea water has to be supersaturated with calcium (Ca_2^+) and carbonate ions (CO_3^{2-}) to form $CaCO_3$:

$$Ca^{2+} + CO_3^{2-} \rightarrow CaCO_3 \qquad (1.4)$$

In undersaturated waters, the shell forming reaction may reverse, and shells may start to dissolve:

$$CaCO_3 + H_2O + CO_2^- \rightarrow Ca^{2+} + 2HCO^{3-} \qquad (1.5)$$

The solubility of calcium carbonate depends on the concentration of CO_3^{2-} (Equation 1.5), therefore indirectly on pH, temperature, and pressure (Fabry et al., 2008). A decrease in CO_3^{2-} reduces the saturation state of $CaCO_3$, which negatively affects shell and skeleton production for some $CaCO_3$ secreting species such as corals (IIPCC, 2001). The reduced concentration of CO_3^{2-} carbonate ions in seawater results in more energy-costly extraction

of the carbonate ion, which is the building block for the shells of $CaCO_3$ secreting species (Equation 1.5). Also, an increased concentration of H^+ ions due to decreased seawater pH makes it energetically more expensive for the $CaCO_3$ secreting species to release H^+ while building shells (Equations 1.2 and 1.5), which may slow down or stop the shell building process (Secretariat of the Convention on Biological Diversity, 2009).

1.4. Ocean acidification (OA) effects on marine organisms and calcification

Carbon transportation in the carbon cycle is partly facilitated by marine organisms that use carbon for the basic processes they need to survive, such as food production (photosynthesis), respiration, and molting.

The effects of OA on marine organisms will vary among species depending on genetics, environmental factors, and adaptive mechanisms (NOAA Ocean Acidification Steering Committee, 2010). In addition to visible OA effects such as shell formation, OA can have behavioral and metabolic impacts on marine species. For example, hypoxia is defined as a decline of oxygen concentration in tissues, and is caused by increased levels of aquatic CO_2. To various degrees, it can reduce respiration, growth, and predation rates (resulting in lethargy and hence decreased predation). Research suggests that fish and crustaceans are most vulnerable, while mollusks, cnidarians, and priapulids are most tolerant (Raven et al., 2005; Vaquer-Sunyer et al., 2008). Published data on corals, coccolithophores, and foraminifera all suggest a reduction in calcification by 5–25% in response to a doubling of atmospheric CO_2 from pre-industrial levels (from 280 to 560 ppm CO_2) (Feely et al., 2004). See Table 1.1 for a list of examples of OA impacts on some marine organisms.

Ocean acidification may impact many species' reproductive potential, growth rates, and susceptibility to disease in addition to its impact on the rate of calcification. Such responses to OA might result in cascading effects throughout the ocean food web, which may change the future of many marine populations, and the dynamics within the marine systems (Raven et al., 2005).

1.5. Conclusions

The global atmospheric concentration of CO_2 has increased from the pre-industrial level of ~280ppm to ~384ppm, leading to approximately a 30% increase in the acidity of the oceans (IPCC, 2007). The rate of change in the ocean pH level is 100 times faster than that was experienced during the last 20 million years (Turley et al., 2007). By 2100, the oceans will be approximately 0.4-0.45 pH units less alkaline (i.e., more acidic, which is a 150-185% increase in acidity, if the trend in CO_2 emissions continues) (Steinacher et al., 2009).

Increasing ocean acidification reduces the availability of carbonate minerals (aragonite and calcite) in seawater that serve to build shells and skeletons for many marine organisms. As the oceans become less saturated with carbonate minerals over time, those marine organisms are likely to experience decreased shell/skeleton building rates, or in the worst cases dissolution. The $CaCO_2$ saturation horizon defines the line

below which shells and skeletons readily dissolve (Feely, et al, 2008). This horizon is shifting upward, and it is predicted that 70% of cold-water corals will be below the saturation horizon by 2100 (Guinotte and Fabry, 2008).

Theory suggests that the effects of ocean acidification will be mainly negative with fewer species benefiting from it, such as some sea grasses (Hall et al., 2008). Ocean acidification is irreversible in short term, and its cumulative effects will profoundly impact the marine ecosystems.

1.6. References

Byrne, M., Ho, M., Selvakumaraswamy, P., Nguyen, H.D., Dworjanyn, S.A., and Davis, A.R. 2009. Temperature, but not pH, compromises sea urchin fertilization and early development under near-future climate change scenarios. Proc. R. Soc. B 276: 1883–1888.

Caldeira, K., and Wickett, M.E. 2003. Anthropogenic carbon and ocean pH. Nature 425: 365.

De'ath, G., Lough, J.M., and Fabricius, K.E. 2009. Declining Coral Calcification on the Great Barrier Reef. Science 323: 116–119.

Doney, S.C., and Schimel, D.S. 2007. Carbon and Climate System Coupling on Timescales from the Precambrian to the Anthropocene*. Ann. Rev. Environ. Res. 32: 31–66.

Dupont, S., Havenhand, J., Thorndyke, W., Peck, L., and Thorndyke, M. 2008. Contribution to the Theme Section "Effects of ocean acidification on marine ecosystems" Near-future level of CO2-driven ocean acidification radically affects larval survival and development in the brittlestar *Ophiothrix fragilis*. Mar. Ecol. Prog. Ser. 373: 285–294.

Fabry, V.J., Seibel, B.A., Feely, R.A., and Orr, J.C. 2008. Impacts of ocean acidification on marine fauna and ecosystem processes. ICES J. Mar. Sci. 65: 414–432.

Feely, R.A., Sabine, C.L., Lee, K., Berelson, W., Kleypas, J., Fabry, V.J., and Millero, F.J. 2004. Impact of Anthropogenic CO2 on the CaCO3 System in the Oceans. Science 305: 362–366.

Feely, R.A., Sabine, C.L., Hernandez-Ayon, J.M., Ianson, D., and Hales, B. 2008. Evidence for Upwelling of Corrosive "Acidified" Water onto the Continental Shelf. Science 320: 1490–1492.

Fine, M., and Tchernov, D. 2007. Scleractinian Coral Species Survive and Recover from Decalcification. Science 315: 1811.

Gattuso, J.-P., Frankignoulle, M., Bourge, I., Romaine, S., and Buddemeier, R.W. 1998. Effect of calcium carbonate saturation of seawater on coral calcification. Global Planet. Change 18: 37–46.

Gazeau, F., Quiblier, C., Jansen, J.M., Gattuso, J.-P., Middelburg, J.J., and Heip, C.H.R. 2007. Impact of elevated CO_2 on shellfish calcification. Geophys. Res. Lett. 34: L07603.

Green, M.A., Jones, M.E., Boudreau, C.L., Moore, R.L., and Westman, B.A. 2004. Dissolution Mortality of Juvenile Bivalves in Coastal Marine Deposits. Limnol. Oceanogr. 49: 727–734.

Guinotte, J.M., and Fabry, V.J. 2008. Ocean Acidification and Its Potential Effects on Marine Ecosystems. Ann. NY Acad. Sci. 1134: 320–342.

Hall-Spencer, J.M., Rodolfo-Metalpa, R., Martin, S., Ransome, E., Fine, M., Turner, S.M., Rowley, S.J., Tedesco, D., and Buia, M.-C. 2008. Volcanic carbon dioxide vents show ecosystem effects of ocean acidification. Nature 454: 96–99.

IPCC, 2001. Climate Change 2001: The Scientific Basis. Contributions of Working Group I to the Third Assessment Report of the Intergovernmental Panel on Climate Change [Houghton, J.T., Ding, D.J. Griggs, M.Nouguer, P.J. van der Linden, and D. Xiaosu (eds.)]. Cambridge University Press, Cambridge, United Kingdom and New York, NY, USA, 881 pp.

IPCC, 2007. Climate Change 2007: The Physical Science Basis. Contribution of Working Group I to the Fourth Assessment Report of the Intergovernmental Panel on Climate Change [Solomon, S., D. Qin, M. Manning, Z. Chen, M. Marquis, K.B. Averyt, M. Tignor and H.L. Miller (eds.)]. Cambridge University Press, Cambridge, United Kingdom and New York, NY, USA, 996 pp.

Langdon, C., Takahashi, T., Sweeney, C., Chipman, D., Goddard, J., Marubini, F., Aceves, H., Barnett, H., and Atkinson, M.J. 2000. Effect of calcium carbonate saturation state on the calcification rate of an experimental coral reef. Global Biogeochem Cy 14: 639–654.

Leclercq, N., Gattuso, J.-P., and Jaubert, J. 2002. Primary Production, Respiration, and Calcification of a Coral Reef Mesocosm under Increased CO_2 Partial Pressure. Limnol. Oceanogr. 47: 558–564.

Maier, C., Hegeman, J., Weinbauer, M.G., and Gattuso, J.-P. 2009. Calcification of the cold-water coral *Lophelia pertusa* under ambient and reduced pH. Biogeosciences 6: 1671–1680.

McDonald, M.R., McClintock, J.B., Amsler, C.D., Rittschof, D., Angus, R.A., Orihuela, B., and Lutostanski, K. 2009. Effects of ocean acidification over the life history of the barnacle *Amphibalanus amphitrite*. Mar. Ecol. Prog. Ser. 385: 179–187.

Michaelidis, B., Ouzounis, C., Paleras, A., and Portner, H.O. 2005. Effects of long-term moderate hypercapnia on acid-base balance and growth rate in marine mussels *Mytilus galloprovincialis*. Mar. Ecol. Prog. Ser. 293: 109–118.

Miller, A.W., Reynolds, A.C., Sobrino, C., and Riedel, G.F. 2009. Shellfish Face Uncertain Future in High CO2 World: Influence of Acidification on Oyster Larvae Calcification and Growth in Estuaries. PLoS ONE 4: e5661.

NOAA Ocean Acidification Steering Committee. 2010. NOAA Ocean and Great Lakes Acidification Research Plan, NOAA Special Report, 143 pp.

Orr, J.C., Fabry, V.J., Aumont, O., Bopp, L., Doney, S.C., Feely, R.A., Gnanadesikan, A., Gruber, N., Ishida, A., Joos, F., Key, R.M., Lindsay, K., Maier-Reimer, E., Matear, R., Monfray, P., Mouchet, A., Najjar, R.G., Plattner, G.-K., Rodgers, K.B., Sabine, C.L., Sarmiento, J.L., Schlitzer, R., Slater, R.D., Totterdell, I.J., Weirig, M.-F., Yamanaka, Y., and Yool, A. 2005. Anthropogenic ocean acidification over the twenty-first century and its impact on calcifying organisms. Nature 437: 681–686.

Parker, L.M., Ross, P.M., and O'connor, W.A. 2009. The effect of ocean acidification and temperature on the fertilization and embryonic development of the Sydney rock oyster *Saccostrea glomerata* (Gould 1850). Global Change Biol. 15: 2123–2136.

Raven, J., Caldeira, K., Elderfield, H., Hoegh-Guldberg, O., Liss, P.S., Riebesell, U., Shepherd, J., Turley, C., and Watson, A.J. 2005. Ocean acidification due to increasing atmospheric carbon dioxide. The Royal Society Policy Document 12/05, London.

Riebesell, U., Zondervan, I., Rost, B., Tortell, P.D., Zeebe, R.E., and Morel, F.M.M. 2000. Reduced calcification of marine plankton in response to increased atmospheric CO_2. Nature 407: 364–367.

Secretariat of the Convention on Biological Diversity. 2009. Scientific Synthesis of the Impacts of Ocean Acidification on Marine Biodiversity. Montreal, Technical Series No. 46, 61 pages.

Shirayama, Y., and Thornton, H. 2005. Effect of increased atmospheric CO_2 on shallow water marine benthos. J. Geophys. Res. 110: C09S08.

Sigler, M.F., Foy, R.J., Short, J.W., Dalton, M., Eisner, L.B., Hurst, T.P., Morado, J.F., and Stone, R.P. 2008. Forecast fish, shellfish and coral population responses to ocean acidification in the north Pacific Ocean and Bering Sea: An ocean acidification research plan for the Alaska Fisheries Science Center. AFSC Processed Rep. 2008-07, 35 p.

Steinacher, M., Joos, F., Froelicher, T.L., Plattner, G.-K., and Doney, S.C. 2009. Imminent ocean acidification in the Arctic projected with the NCAR global coupled carbon cycle-climate model. Biogeosciences 6: 515–533.

Turley, C., Roberts, J., and Guinotte, J. 2007. Corals in deep-water: will the unseen hand of ocean acidification destroy cold-water ecosystems? Coral Reefs 26: 445–448.

Vaquer-Sunyer, R., and Duarte, C.M. 2008. Thresholds of hypoxia for marine biodiversity. P. Natl. Acad. Sci. 105: 15452–15457.

1.7. Tables

Table 1.1 Ocean acidification impacts on some organism.

Organism	Lower pH impact	Source
Planktonic organisms	Decrease in calcification rates (25-40%); structural damage in shells in coccolithophores	(Riebesell et al., 2000)
	Shell dissolution in living pteropods (for the level of carbonate content of the ocean expected in the next 50 years)	(Freely et al., 2004)
Corals (warm and cold* water)	14.2% decrease in coral calcification rates observed on the Great Barrier Reef	(De'ath et al., 2009)
	Two stony Mediterranean corals *Oculina patagonica* and *Madracis pharencis* maintained under low pH underwent complete skeleton dissolution, but maintained health and recovered once returned to ambient conditions	(Fine et al., 2007)
	Negative impact on shell and skeleton production in some coral species	(IPCC, 2001).
	Decline in calcification rates linked to carbonate saturation state	(Leclercq et al., 2002)
	59% reduction in calcification rates observed in juvenile deep sea coral *Lophelia pertusa* compared with older polyps	(Maier et al., 2009)
Echinoderms (sea stars, sea urchins, sand dollars, and sea cucumbers)	Reduction in growth rates, size and body weight	(Michaelidis et al., 2005)
	Test (shell) dissolution	(Shirayama et al., 2005)
	Abnormal morphology in pluteus larvae reducing competitive advantage. Brittlestar *Ophiothrix fragilis*, a keystone species of shelf seas in north-western Europe, showed 100% larval mortality when pH was decreased by 0.2 units.	(Dupont et al., 2008)
	H. erythrogramma fertilization and early development was observed to be robust to decreased pH within predicted values for environmental change.	(Byrne et al., 2009)
	Lower rate of shell calcification	(Gazeau et al., 2007)

Molluscs	Juvenile clams *Mercenaria mercenari*a showed substantial shell dissolution and increased mortality.	(Green et al., 2004)
	Fertilization in Sydney rock oyster *Saccostrea glomerata* was reduced as a result of CO2 increase and temperature change from optimum.	(Parker et al., 2009)
	16% decrease in shell area and a 42% reduction in calcium content in oyster *Crassostrea virginica* grown in estuarine water under simulated pCO2 regimes comparing pre-industrial to 2100. *Crassostrea ariakensis* larvae showed no change to either growth or calcification under the same treatments.	(Miller et al., 2009)
Crustaceans	No observed effect of reduced pH on barnacle *Amphibalanus Amphitrite* larval condition, cyprid (final larval stage) size, cyprid attachment and metamorphosis, juvenile to adult growth, or egg production.	(McDonald et al., 2008)
	Reduced calcification rates.	(Gattuso et al., 1998) (Langdon et al., 2000) (Riebesell et al., 2000)
Sea grasses close to CO_2 vents.	Thrive or are resilient.	(Hall et al., 2008)

Chapter 2: Ocean acidification impact on Bristol Bay Red king crab recruitment

2.1 Introduction

2.1.1 Bristol Bay Red King Crab (BBRKC)

Red king crab (*Paralithodes camtschatica*) was historically one of the most valuable shellfish resources on Alaska's Continental Shelf. A record 128.1 million lbs (58,101 t; $115.3 million in revenue) of red king crab (RKC) was harvested by U.S. fishers during the 1980-81 fishing season, whereas landings during 2010 were only 13.3 million lbs (6,010 t; and $83.2 million in revenue) (Zheng and Siddeek, 2010; Fitch et al., 2012). The NMFS survey data implies that a decline in abundance occurred suddenly during the early 1980s. The landings have remained low since 1982 (Fig. 2.1). A combination of high exploitation rates, high natural mortality with low and variable year-class strength, predation by fish on eggs, and microsporidian diseases (Jewett and Onuf, 1988) has been suggested to have contributed to the decline.

Zheng and Kruse (2006) noted that the abundances of Eastern Bering Sea (EBS) crab stocks, including red king crab in Bristol Bay (BBRKC), are driven by recruitment variability. In a closed population, abundance increases through recruitment and decreases due to catch and natural mortality. When recruitment exceeds catch and natural mortality, abundance increases and *vice versa*.

Spawning biomass can explain some of the variation in recruitment through a stock recruitment relationship when recruitment is density-dependent (e.g. Ricker, 1954; Beverton and Holt, 1957). The remaining variation is due to environmental factors such

as temperature, wind, barometric pressure, food availability, and survival rates, etc.; all of which are hypothesized to impact recruitment strength (Shepherd et al., 1984). In a 4-year study in Auke Bay, Alaska, Shirley and Shirley (1990) found that larval survival was inversely related to the duration of the larval stage suggesting that longer larval stages lead to reduced larvae survival rate. Zheng and Kruse (2003) argued that BBRKC has the strongest density-dependent stock-recruitment relationship among all crab stocks in the EBS. However, Zheng and Kruse (2003) also found a high correlation among decadal recruitment, and argued that this implies an environmental influence on BBRKC recruitment.

This chapter focuses on modeling the potential consequences of OA on crab populations through its impact on crab recruitment and growth. OA may slow down the process of shell construction in molting crab, which may reduce larval growth and fitness (Walther et al., 2010). Survival of pre-recruitment stages and their growth rates are modeled in this chapter under four OA scenarios, and trends in recruitment to the first size-classes in the stock assessment model for BBRKC are estimated.

2.1.2 Life history, survival, and growth rates in BBRKC

Crab life history consists of two distinct stages, a short pelagic stage followed by a protracted benthic stage (Jewett and Onuf, 1988). Adult red king crabs conduct two migrations annually: a mating-molting migration and a feeding migration. During the mating-molting migration, adults migrate to shallow waters (<50m) to mate and spawn during spring. They move to deeper waters in the summer and fall to feed (Jewett and Onuf, 1988). Gravid females carry eggs for approximately 11 months before they hatch. The exact date of hatching is largely determined by the timing of breeding for primiparous vs. multiparous females (Jewett and Onuf, 1988) and the length of the incubation time, which is influenced by the water temperature (Shirley and Shirley, 1989). The onset of hatch, and hence the occurrence of pelagic larvae, can vary by as much as 4-6 weeks from time of spawning (Jewett and Onuf, 1988; Loher et al., 2001). Thus, larval red king crabs are found in Bristol Bay from April to August.

The pre-zoeal larvae molt within minutes into the zoeal form upon hatching. The pelagic zoeae go through five stages: four zoeal stages each lasting 10-14 days, and a glaucothoe stage, which is sometimes referred to as the megalopa stage. Zoeal stages are characterized by numerous molts. Crab in the glaucothoe stage start to resemble adult crab. This last planktonic stage lasts about 18-56 days, after which animals molt and settle in their first benthic instar crab stage. No feeding occurs during the glaucothoe stage. Crabs in this stage use all of their energy to find the best benthic habitat (i.e. habitat abundant in food and shelter), which increases their chances of survival through the juvenile stages.

Juvenile red king crabs are solitary during their first year of life and use rocks or the epifaunal community for shelter. Survival during the first benthic stage as juveniles depends highly on the availability of shelter (Pirtle and Stoner, 2010). Dependence on the benthic habitat ends during the second year when juveniles migrate to deeper water (20-50m), and begin to “pod”, or congregate, in large tightly packed groups.

Podding continues until about four years of age (about 65 mm CL) when the juvenile crab move to deeper water and join the adults (Loher et al., 1998). The pelagic larvae consume phytoplankton and zooplankton. Once settled in deeper water, they feed on the dominant epifauna, which they also use as shelter. Small crabs can feed on sea stars, kelp, molted king crab exuvia, clams, mussels, nudibranch egg masses, and barnacles, whereas adults are opportunistic omnivores (Loher et al., 1998).

Accurate growth rates are needed to determine the time lag between spawning and subsequent recruitment to the fishable population (Loher et al., 2001). The commonly accepted age to reproductive maturity of the RKC is seven years (Zheng et al., 1995a, 1995b), and seven years is also used as the age at which RKC are assumed to recruit in the stock assessment model. Alternatively, Loher et al. (2001) suggest that red king crab in Bristol Bay are likely to reach the recruitment size in the stock assessment model at around 8 and 9 years after settlement. This chapter assumes seven years to recruitment, which is consistent with the RKC stock assessment model.

2.2 Methods

2.2.1 Introduction to the pre-recruitment model

The dynamics of pre-recruitment red king crab is governing by the equation:

$$\underline{N}_{T+t+1} = \mathbf{G}_T \mathbf{\Omega}_T \underline{N}_{T+t} \tag{2.1}$$

where N_{T+t} is the vector of numbers-at-length at time T+t (the numbers-at-length at time T are the number of eggs spawned, represented as a 1 in the first size-class and zeros in the remaining size-classes), $\mathbf{G}_T$ is the growth matrix (i.e. the matrix of probabilities of growing from one size-class to each other size-class) for eggs spawned at time T, and Ω_T is the survival matrix for eggs spawned at time T. The last size-class in this model is the first size-class in the stock assessment model (67.5 mm CL; Zheng and Siddeek, 2010). Projections of Equation 2.1 are conducted under various ocean acidification scenarios defined by different levels of the ocean pH (see Fig. 2.2 for a flowchart of the process).

The vector $\underline{N}$ consists of 18 pre-recruitment stages (4 zoeal stages, 1 glaucothoeal, and 13 juvenile stages, denoted Z1-Z4, G, C1-C8, and J1-J5) (Table 2.1), with each stage divided into a number of sub-stages to implement a minimum time in each stage. The stages with the shortest durations, the zoeal stages, last on average 12 days (Table 2.2). Half of the average zoeal stage duration is used to define the time (t) step for the model [6 days]. It is assumed that all individuals within a stage are subject to the same survival probability and stage duration, and that individuals must stay in a stage for at least a defined minimum amount of time (Table 2.2) before progressing to the next stage.

The matrix $\mathbf{G}_T \mathbf{\Omega}_T$ determines the combined effects of growth and mortality. This matrix can be written as:

$$\Sigma_T = \begin{pmatrix} 0 & 0 & 0 & 0 & 0 & ... \\ S_{1,T} & S_{1,T}(1-P_{1,T}) & 0 & 0 & 0 & ... \\ 0 & S_{1,T}P_{1,T} & 0 & 0 & 0 & ... \\ 0 & 0 & S_{2,T} & S_{2,T}(1-P_{2,T}) & 0 & ... \\ 0 & 0 & 0 & S_{2,T}P_{2,T} & 0 & ... \\ 0 & 0 & 0 & 0 & S_{3,T} & .. \\ 0 & 0 & 0 & 0 & 0 & ... \end{pmatrix} \quad (2.2)$$

for the case in which animals must stay at least one time-step in stages 1-4. $S_{i,T}$ is the probability of survival for stage *i* for animals spawned at time *T*, and $P_{i,T}$, is the probability of growing out of stage *i* for animals spawned at time *T*.

The values for the $S_{i,T}$ and $P_{i,T}$ are solved for to match values for the expected duration ($\tilde{d}_{i,T}$) and estimated expected survival ($\tilde{S}_{i,T}$) for stage *i* for eggs spawned at time *T*. The predicted values for $\tilde{S}_{i,T}$ and $\tilde{d}_{i,T}$ for a stage with *n* sub-stages are:

$$\tilde{S}_{i,T} = \frac{S_{i,T}^n P_{i,T}}{1 - S_{i,T}(1-P_{i,T})}; \quad \tilde{d}_{i,T} = \sum_{y=T}^{T+tt} (y+1) x_{i,y} S_{i,T} P_{i,T} / \sum_{y=T}^{T+tt} x_{i,y} S_{i,T} P_{i,T} \quad (2.3)$$

where $x_{i,y}$ is the number of animals leaving the stage *i* at time step *T* (for stage 1, this would be the numbers entering stage 2 in Equation 2.2), and *tt* is the number of time-steps in the model (*tt*~1100). The derivation of Equation (2.3) is given in Appendix 2.A.

The expected stage survivals ($\tilde{S}_i$) are selected given the overall expected survival (SS = 0.0000046) from egg to subsequent recruitment inferred from the stock assessment (Zheng and Siddeek, 2010). In addition, the survival rates for the stages covered by the NMFS Kodiak experiment (C1-C8) were tuned to equal the survival for the controls in the experiment (see Table 2.2 for expected stage survivals). The survival for a given stage is density-independent, and depends on the number of molts during that stage (mt_i), described by $\tilde{S}_i = e^{-\lambda mt_i}$ where the value of the scaling parameter λ is selected so that $SS = \prod_{i=1}^{18} \tilde{S}_i$.

2.2.2 Survival rates and duration times as functions of pH

Survival rates for each pH level are calculated based on a linear relationship between ocean pH and survival rate:

$$\tilde{S}_{i,T} = \tilde{S}_i (1 - \gamma * \frac{|\,\mathrm{pH}_T - \mathrm{pH}\,|}{\mathrm{pH}}) \quad (2.4)$$

where, $\tilde{S}_{i,T}$ is the survival rate for the animals in stage *i* that were spawned at time *T*, $\tilde{S}_i$ is the reference (non-OA impacted) survival rate for stage *i*, γ is the slope of the linear relationship, pH is the reference OA-neutral pH value, and pH_T is the ocean pH value at time *T*. Stage duration times for each pH level are calculated based on a linear relationship between ocean pH and stage duration:

$$\tilde{d}_{i,T} = \tilde{d}_i (1 - \alpha * \frac{|pH_T - pH|}{pH}) \quad (2.5)$$

where, $\tilde{d}_{i,T}$ is duration of stage *i* for the animals which were spawned at time *T*, $\tilde{d}_i$ is the is the reference (non-OA impacted) duration for stage *i*, and α is the slope of the linear relationship.

2.2.3 Parameterization

Changes over time in pH were calculated by fitting a straight line to the predictions of pH levels in the ocean between 2000 and 2200; pH_{2000}=8.1, pH_{2200}=7.4 (Hall-Spencer et al., 2008; Caldeira and Wickett, 2003), where the unit for time *k* is 1 year.

$$pH_{(t)} = 8.1 + (7.4\text{-}8.1)(k\text{-}1)/(200) \quad (2.6)$$

Uncertainty is accounted for by conducting 100 simulations where the reference values for annual survival and stage duration are drawn independently from beta and uniform distributions, respectively (see Table 2.3 for a summary of the distributions concerned). The beta distribution was defined by shape parameters which were calculated from average values and standard deviations for the survival values. The standard deviations were assumed to be 0.1 (in the absence of data on the variance in average survival). Stage duration times were obtained from Kovatcheva et al. (2006) for the first five stages, Donaldson et al. (1992) for stages 6-13, and Lohr et al. (2001) for stages 14-18 (Table 2.1). Each simulation involves drawing stage durations from the uniform distributions defined by the earliest and latest stage end times (Table 2.1).

2.2.4 Scenarios

The impact of OA on recruitment is explored using 16 scenarios in which the values for α and γ change (Equations 2.4 and 2.5). The base scenario (α=0; γ=0) corresponds to no OA impact on the dynamics of red king crab, while the other scenarios (based on values for α of 3.33, 6.67, and 10, and values for γ of -3.33, -6.67, and -10) explore impacts of increasing OA on stage duration and survival, respectively.

2.3 Results

The impact of OA is quantified as the relative difference in the median number of crabs recruited to the model given a constant egg production, and the relative change in the average time between spawning and recruitment to the smallest size-class in the assessment model. Deterministic and stochastic projections are considered for the 16

scenarios. The deterministic results allow broad features of the results to be identified while the stochastic results allow the impact of uncertainty to be quantified.

2.3.1 Deterministic results

The zero-zero combination for α and γ ($\alpha = 0; \gamma = 0$) corresponds to the scenario in which OA has no impact on survival and stage duration times (Figure 2.3, first column). Survival and time to recruitment are constant over time for this scenario, as expected. The remaining plots in the first row of Figure 2.3 show the impact of OA when growth is fixed (i.e. stage duration times are time-invariant; α = 0), and the survival rates decrease over time (γ=0, -3.33, -6.67, -10).Time to recruitment remains constant in this case, and recruitment decreases with decreasing survival. In contrast, time to recruitment increases, and the number of crab recruited remains constant, when stage durations increase over time ($\alpha > 0$), and the survival rates are time-invariant ($\gamma = 0$) (Figure 2.3, second row). OA has the largest negative effect on the number of crab eventually recruiting in scenarios with increasing stage duration times and decreasing survival rates (Figure 2.3: third row). As expected, the most extreme values for the parameters (α = 10; γ = -10) lead to the longest time to recruitment and the lowest pre-recruit survival.

Figure 2.4 summarizes the deterministic 200-year projections (2000–2200) for the percentage of eggs that recruit, and the time to recruitment for all 16 scenarios. The percentage of eggs recruited and the average time-to-recruitment relative to the no OA-impact scenario for eggs spawned in 2041, 2081, 2121, 2161, and 2200 in Figure 2.4 are listed in the Tables 2.4a and 2.5a. Tables 2.4b and 2.5b list stage survival probabilities ($\tilde{S}_i$) and the probabilities of growing out of each stage (P_i) for a sample of six stages for the scenarios in the first two rows of Figure 2.3. The time to recruitment (Figure 2.4 left panel) and the percentage of eggs which recruit (Figure 2.4 right panel), are, as expected, independent of time in the absence of OA (α = 0; γ = 0).

2.3.2 Stochastic Results

Time to recruitment is independent of γ under the stochastic projections, and it increases as the impact of OA on pre-recruit crab stage durations (quantified by α) increases (Figure 2.5). The impact of drawing the reference stage duration from the uniform distribution is relatively small (note the narrow 95% intervals in Figure 2.5). Figure 2.6 shows the results of the stochastic 200-year projections for the percentage of eggs which progress to recruitment under the stochastic projections match the deterministic expectations (Figure 2.6). However, the impact of a standard error of 0.1 on survival leads to marked variation in the percent of eggs that recruit over time (Figure 2.6).

2.3.3 NMFS Kodiak Laboratory research results vs. model results

The results from the NMFS Kodiak Laboratory research on the impact of pH on juvenile red king crab (Long et al., in press) are compared with the results from the model (Figure 2.7). The Kodiak experiment involved two treatments (pH = 7.8, and 7.5) and one control (pH= 8.0). The treatment levels in the experiment correspond to eggs spawned in 2088 and 2159 in the model, respectively. In the experiment, ninety red king crabs were randomly assigned to three tanks, with 30 crabs per tank, and the tanks were randomly

assigned one of the two treatments or the control. The total experimental duration was 192 days, when the time between subsequent moltings became too long (1 year).

Figure 2.7 shows the survival of the modeled crab vs. the survival of the experimental juvenile red king crab. The model results are shown for different rates of survival (γ), and the OA-neutral value for α (0) because survival is independent of α in the model, and the Kodiak experiments do not provide information on stage durations.

The model and the Kodiak experiment results agree for the no-OA scenario for a pH of 8.0 (top left plot in Figure 2.7), which was expected because the reference survival rates in the model were set to match the control survival rates in Kodiak experiment (Equation 2.4). The model results for the mildest impact of OA (γ=-3.3) best match the results of the experiment with pH = 7.8 while the other two modeled OA scenarios (γ=-6.67 and γ=-10) project lower survival rates. The model results are most similar to the experimental results for pH = 7.5 when the impact of OA is based on the largest value considered for γ of -10; otherwise, the survival rates are higher than those observed during the experiment for a pH of 7.5 (lower left plot in Fig. 2.7).

2.4 Discussion

Ocean acidification is predicted to impact crab populations in many ways. Ultimately, it will decrease survival and lead to changes in growth rates by altering physiology, reducing and altering food supply, and changing the environment and species with which the crab interact (Raven et al., 2005). Crab survival and recruitment is not only closely related to growth, but also to the timing between the population and environmental processes. Red king crab spawn in the spring immediately after the females molt (Jewett and Onuf, 1988), and after both male and female crab have migrated to the spawning grounds. Spawning success could be negatively impacted if molting in females is delayed because the time females and males spend together at the spawning grounds is limited. The importance of potential discrepancies in timing between events in RKC life history and the supporting environmental conditions have not yet been investigated.

This model takes a concise approach to modeling OA impacts, allowing other potential impacts to be accounted for under the umbrella of the two main factors addressed by the model (γ and α), and leads to results that demonstrate the consequences of OA (a) on survival of pre-recruit crab and (b) on the growth of these crab. The two effects are separated in the model so that their impacts can be predicted independently and compared with observations were they to be available. This construct allows for estimation of recruitment under various OA scenarios, with possibility of independently turning off and on either of the two main OA effects.

This chapter estimates a range for crab recruitment under 16 OA scenarios for 200 years (2000 - 2200). The predicted fraction of crab surviving differs somewhat between the observations and model predictions for the experimental scenarios in which pH was reduced. The model slightly under-estimates survival for a pH of 7.8 and over-estimates it for a pH of 7.5. The less extreme survival predictions from the model might be more realistic than the laboratory results, had the animals been given time to acclimatize to lower pH's. The short duration of the experiment and the rapid change in pH has not allowed for the crab to adapt to OA. Furthermore, none of the crab in the experiment

hatched from already OA-impacted parents, i.e., the experiment did not allow for selection to act on at least one generation of OA-impacted crab. This may lead the experiments to over-estimate the impact of lower pH on survival if adaptation would occur, or to underestimate the impact. Potential larger cumulative negative OA impacts that might affect RKC independent of survival, such as lower availability of food and a lower ability to move and locate prey due to hypercapnia were not included in laboratory conditions. The actual survival rates would be lower in that case, i.e., the negative consequences of OA on crab would be higher than the model predicts.

Density dependence is another factor that likely impacts larval and juvenile survival rates because survival will depend on finding good shelter and food during the first benthic stage, and the probability of finding good shelter will decline with increasing abundance. Changes in density dependence under OA are expected, but unknown. Data or precise insights into how density dependence impacts pre-recruit survival are, however, not available. The pre-recruitment model focuses on estimation of pre-recruitment survival rates to match overall pre-recruit survival rate deduced from the stock assessment model guided by the results from the Kodiak Laboratory research, and it does not include density-dependence during the pre-recruit stage. Such density-dependence would tend to mitigate the impact of OA reduction of survival. Density dependence in post-recruit dynamics is accounted for in the population model using a Ricker stock-recruitment relationship.

Ideally, future research on the impact of reduced pH on crab would: (1) include pH values predicted from now until at most 2050, and consider pH values in smaller steps between current and the future values; (2) the treated animals would be a group of mature females with a group of males (juvenile and mature) to allow mating to occur, where the ratio of females to mature males mimics that estimated for the actual population of red king crab; and (3) the experiment would be conducted over at least 2-3 years.

Such experimental design would allow more precise estimation of survival rates under OA scenarios relevant to the next 50 years, and at the same time address several other questions: (1) what is the response of crab growth and survival to smaller incremental changes in pH; (2) what is the impact of OA on fecundity and fertilization rates due to hypercapnia and potential changes in behavior; (3) is there a change in the quality of fertilized eggs, as quantified using for example fat content, given OA conditions; (4) what are the survival and growth rates of 2nd and 3rd generation larvae and juvenile crab hatched in OA conditions; and (5) are the results constant over time given a constant pH, i.e., do animals adapt or does their ability to resist any negative impacts of OA deteriorate more rapidly than predicted from the current experiments. A major additional benefit of this research would be a greater understanding of the spawning behavior of red king crab and their fertilization success under a high female to male ratio (as is currently estimated by the stock assessment model).

2.5 References

Beverton, R.J.H., and Holt, S.J. 1957. On the Dynamics of Exploited Fish Populations. Fishery Investigations, Ser. 2, Vol. 19, UK Ministry of Agriculture, Fisheries and Food, London.

Caldeira, K., and Wickett, M.E. 2003. Anthropogenic carbon and ocean pH. Nature 425: 365–365.

Donaldson, W.E., Beyersdorfer, S.C., Pengilly, D, and Blau, S.F. 1992. Growth of red king crab, Paralithodes camtschaticus (Tilesius, 1815), in artificial habitat collectors at Kodiak, Alaska. J. Shellfish Res. 11: 85–89.

Fitch, H., Schwenzfeier, M., Baechler, B., Hartill, T., Salmon, M., Deiman, M., Evans, E., Henry, E., Wald, L., Shaishnikoff, J., Herring, K., and Wilson, J. 2012. Annual management report for the commercial and subsistence shellfish fisheries of the Aleutian Islands, Bering Sea and the Westward Region's shellfish observer program, 2010/11. Alaska Department of Fish and Game, Fishery Management Report No. 1222, Anchorage.

Jewett, S.C., and Onuf, C.P. 1988. Habitat suitability index models: red king crab. U.S. Fish Wildlife Service Biological Report 82: 10-153.

Kovatcheva, N., Epelbaum, A., Kalinin, A., Borisov, R., and Lebedev, R. 2006. Early life history stages of the red king crab *Paralithodes camtschaticus* (Tilesius, 1815): biology and culture. VNIRO Publishing, Moscow.

Hall-Spencer, J.M., Rodolfo-Metalpa, R., Martin, S., Ransome, E., Fine, M., Turner, S.M., Rowley, S.J., Tedesco, D., and Buia, M.C. 2008. Volcanic carbon dioxide vents show ecosystem effects of ocean acidification. Nature 454: 96–99.

Loher, T., Hill, P.S., Harrington, G., and Cassano, E. 1998. Management of Bristol Bay Red King Crab: A Critical Intersections Approach to Fisheries Management. Rev. Fisher. Sci. 6: 169–251.

Loher, T., Armstrong, D.A., and Stevens, B.G. 2001. Growth of juvenile red king crab (*Paralithodes camtschaticus*) in Bristol Bay (Alaska) elucidated from field sampling and analysis of trawl-survey data. Fish. B.-NOAA. 99: 572–587.

Long W.C., Swiney, K.M., Harris, C., Page, H.N., and Foy, R.J. 2013. Effects of ocean acidification on juvenile red king crab (*Paralithodes camtschaticus*) and Tanner crab (*Chionoecetes bairdi*). Kodiak Laboratory, Resource Assessment and Conservation Engineering Division, Alaska. FSC, NMFS, NOAA. (in press)

Pirtle, J.L., and Stoner, A.W. 2010. Red king crab (*Paralithodes camtschaticus*) early post-settlement habitat choice: Structure, food, and ontogeny. J. Exp. Mar. Biol. Ecol. 393: 130–137.

Raven, J., Caldeira, K., Elderfield, H., Hoegh-Guldberg, O., Liss, P.S., Riebesell, U., Shepherd, J., Turley, C., and Watson, A.J. 2005. Ocean acidification due to increasing atmospheric carbon dioxide. The Royal Society Policy Document 12/05, London.

Ricker, W.E., 1954. Stock and Recruitment. J. Fish. Res. Board Can. 11: 559–623.

Shepherd, J.G., Pope, J.G., and Cousens, R.D. 1984. Variations in fish stocks and hypotheses concerning their links with climate. Rapp. P.-v Reun. Cons. Int. Expl. Mer 185: 255–267.

Shirley, S., and Shirley, T. 1989. Interannual Variability in Density, Timing and Survival of Alaskan Red King Crab Paralithodes-Camtschatica Larvae. Mar. Ecol. Prog. Ser. 54: 51–59.

Shirley, T.C., and Shirley S.M. 1990. Planktonic survival of red king crab larvae in a subarctic ecosystem, 1985–1989. pp. 263–285. In: APPRISE – Interannual variability and fisheries recruitment, Ziemann, D.A., and Fulton-Bennet, K.W., (eds.) The Oceanic Institute, Hawaii, USA.

Walther, K., Anger, K., and Prtner, H.O. 2010. Effects of ocean acidification and warming on the larval development of the spider crab Hyas araneus from different latitudes (54° vs. 79°N). Mar. Ecol. Prog. Ser. 417: 159–170.

Zheng, J., Murphy, M.C., and Kruse, G.H.1995a. A length-based population model and stock-recruitment relationships for red king crab, *Paralithodes camtschaticus*, in Bristol Bay. Can. J. Fish. Aquat. Sci. 52: 1229–1246.

Zheng, J., Murphy, M.C., and Kruse, G.H. 1995b. Updated length-based population model and stock recruitment relationship for red king crab in Bristol Bay, Alaska. Alaskan Fish. Res. Bull. 2: 114–124.

Zheng, J., and Kruse, G.H. 2003. Stock-recruitment relationships for three major Alaskan crab stocks. Fish. Res. 65: 103–121.

Zheng, J., and Kruse, G.H. 2006. Recruitment variation of eastern Bering Sea crabs: Climate-forcing or top-down effects? Prog. Oceanogr. 68: 184–204.

Zheng, J., and Siddeek, M.S.M. 2010. Bristol Bay red king crab stock assessment in fall 2010. In: Stock Assessment and Fishery Evaluation Report for the King and Tanner Crab Fisheries of the Bering Sea and Aleutian Islands Region: 2010 Crab SAFE. North Pacific Fishery Management Council, Anchorage.

2.6 Tables and figures

Table 2.1 Stage durations for Bristol Bay red king crab.

Stage	Duration	Molts	CL (mm)	Source
Z1-Z4	10-14 days	1	1.18-2.07	(Kovatcheva et al. 2006)
G	18-56 days	1	1.8-2.0	(Kovatcheva et al. 2006)
C1 –C8	20-30 days	1	2.18 -9.5	(Donaldson et al. 1992)
J1	365 days	3	9-22	(Lohr et al. 2001)
J2	365 days	2	23-46	(Lohr et al. 2001)
J3-J4	365 days	1	47-62	(Lohr et al. 2001)
J5	174 days	1	63-67.5	(Lohr et al. 2001)

Table 2.2. Average stage durations and minimum times spent in stages, and overall expected stage survivals.

Stage	Average Duration	Minimum Time Spent in Stage	Expected stage survival ($\tilde{S}_i$)
Z1	12 days	10	0.10503
G	37 days	18	0.10503
C1 –C8	25 days	20	0.93814
J1	365 days	365	0.82567
J2	365 days	365	0.88011
J3-J4	365 days	365	0.93814
J5	174 days	174	0.93814

Table 2.3. Distributions for annual survival and stage duration times.

Parameter	Distribution	Equation
Annual Survival	Beta	$f(x;\alpha,\beta) = \frac{1}{B(\alpha,\beta)} x^{\alpha-1}(1-x)^{\beta-1}$ $\hat{\alpha} = \tilde{S}(\frac{\tilde{S}(1-\tilde{S})}{v} - 1)$ $\hat{\beta} = (1-\tilde{S})(\frac{\tilde{S}(1-\tilde{S})}{v} - 1)$
Stage Duration Times	Uniform	$f(x) = \frac{1}{B-A}$ $A \le x \le B$

Table 2.4a. Percentage change in recruitment [percentage of spawned eggs which recruit] for various values of γ relative to the no OA ($\alpha = 0$ and $\gamma = 0$) scenario for five spawning years. The number of eggs recruited is independent of α.

γ	**2041 [%]**	**2081 [%]**	**2121 [%]**	**2161 [%]**	**2200 [%]**
-3.3	35.44	12.56	4.45	1.58	0.58
-6.7	12.56	1.58	0.20	0.02	0.00
-10	4.45	0.20	0.01	0.00	0.00

Table 2.4b. Change in survival probabilities for six stages for various values of γ, where $\alpha = 0$ relative to the no OA ($\alpha = 0$ and $\gamma = 0$) scenario for five spawning years.

	Survival probability ($\tilde{S}_i$)				
	2041	**2081**	**2121**	**2161**	**2200**
γ= -3.33					
Z1	0.587	0.585	0.583	0.581	0.579
G	0.774	0.772	0.771	0.769	0.767
C1	0.983	0.977	0.972	0.966	0.961
J1	0.996	0.996	0.996	0.995	0.995
J2	0.998	0.997	0.997	0.996	0.996
J5	0.997	0.995	0.995	0.994	0.993
γ= -6.66					
Z1	0.585	0.581	0.577	0.573	0.569
G	0.772	0.769	0.766	0.762	0.759
C1	0.977	0.967	0.956	0.946	0.936
J1	0.996	0.995	0.994	0.993	0.992
J2	0.997	0.996	0.995	0.994	0.993
J5	0.996	0.994	0.992	0.990	0.989
γ= -10					
Z1	0.583	0.577	0.571	0.566	0.561
G	0.771	0.766	0.761	0.756	0.752
C1	0.972	0.957	0.941	0.926	0.911
J1	0.996	0.994	0.993	0.992	0.990
J2	0.997	0.995	0.994	0.993	0.991
J5	0.995	0.992	0.989	0.987	0.984

Table 2.5a. Percentage change in the time to recruitment [years] for various values of α relative to the no OA ($\alpha = 0$ and $\gamma = 0$) scenario for five spawning years. The time to recruitment is independent of γ.

α	**2041 [%]**	**2081 [%]**	**2121 [%]**	**2161 [%]**	**2200 [%]**
3.33	105.61	111.56	117.86	124.53	131.24
6.67	111.56	124.53	139.08	155.34	171.77
10	117.86	139.09	163.98	188.81	202.64

Table 2.5b. Change in stage duration times for six stages for various values of α, where γ = 0 relative to the no OA (α = 0 and γ = 0) scenario for five spawning years.

	Growth probability (P_i)				
	2041	**2081**	**2121**	**2161**	**2200**
α = 3.33					
Z1	0.134	0.119	0.106	0.396	0.319
G	0.211	0.160	0.124	0.197	0.148
C1	0.410	0.369	0.333	0.442	0.388
J1	0.068	0.064	0.060	0.059	0.054
J2	0.069	0.065	0.061	0.060	0.055
J5	0.131	0.118	0.119	0.119	0.104
α = 6.66					
Z1	0.120	0.400	0.261	0.177	0.125
G	0.163	0.200	0.114	0.122	0.121
C1	0.371	0.446	0.344	0.384	0.291
J1	0.065	0.056	0.052	0.046	0.041
J2	0.066	0.057	0.053	0.047	0.042
J5	0.119	0.107	0.103	0.093	0.081
α = 10					
Z1	0.107	0.264	0.149	0.268	0.137
G	0.127	0.116	0.167	0.113	0.113
C1	0.337	0.346	0.335	0.303	0.259
J1	0.062	0.053	0.043	0.038	0.032
J2	0.062	0.054	0.044	0.039	0.032
J5	0.122	0.104	0.089	0.075	0.066

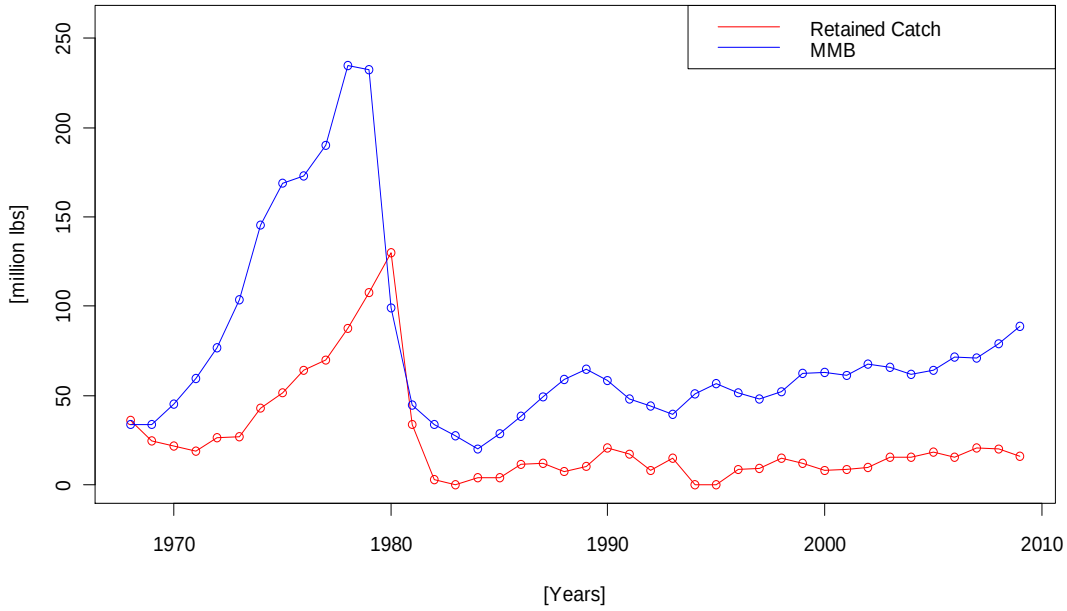

Figure 2.1. Bristol Bay red king crab annual catch and mature male biomass (MMB) (million lbs) for each season (June 1 - May 31) (Zheng and Siddeek, 2010)

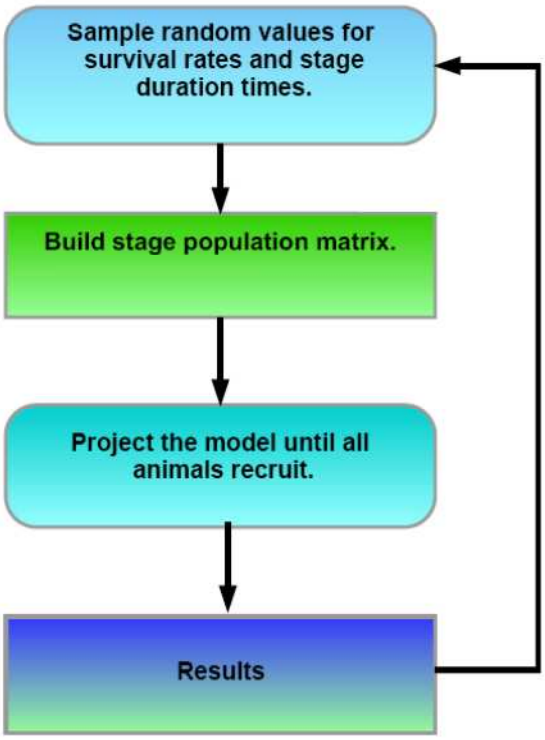

Figure 2.2. Flowchart of the methods.

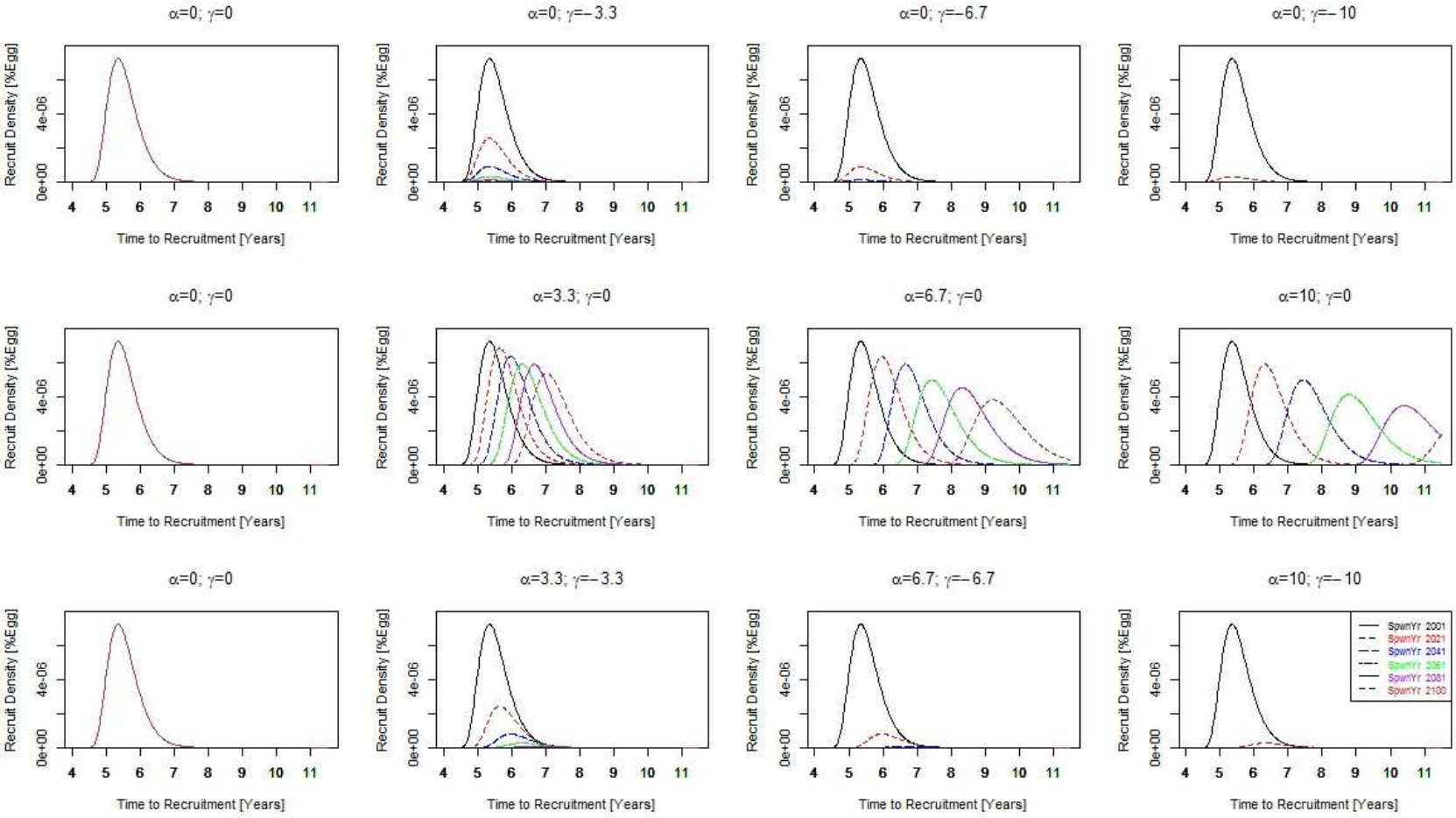

Figure 2.3. Density plot of recruitment [percentage of eggs recruited] and time to recruitment [years] for deterministic simulations in six future years.

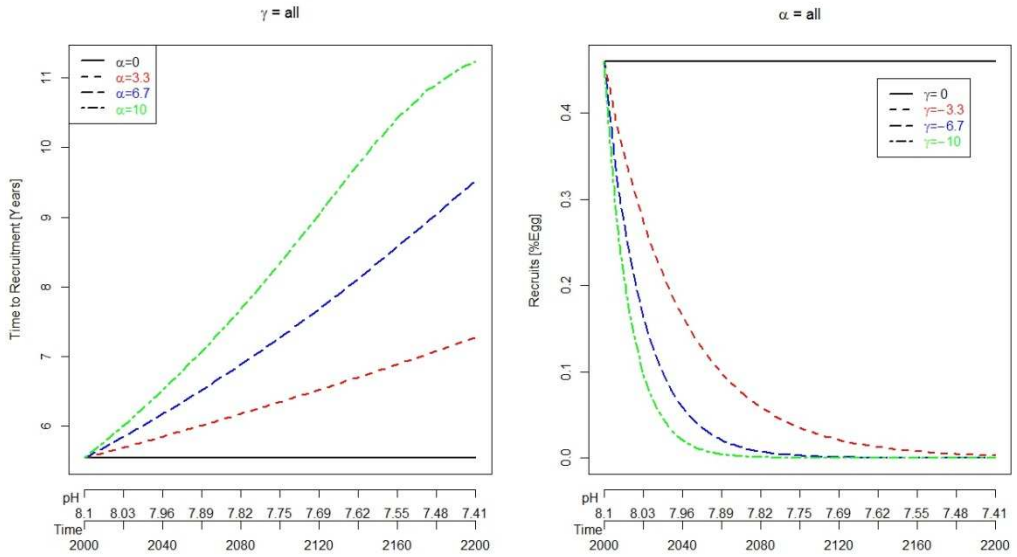

Figure 2.4. Time to recruitment [years] and percent of eggs recruited and for eggs spawned in each year from 2000-2200.

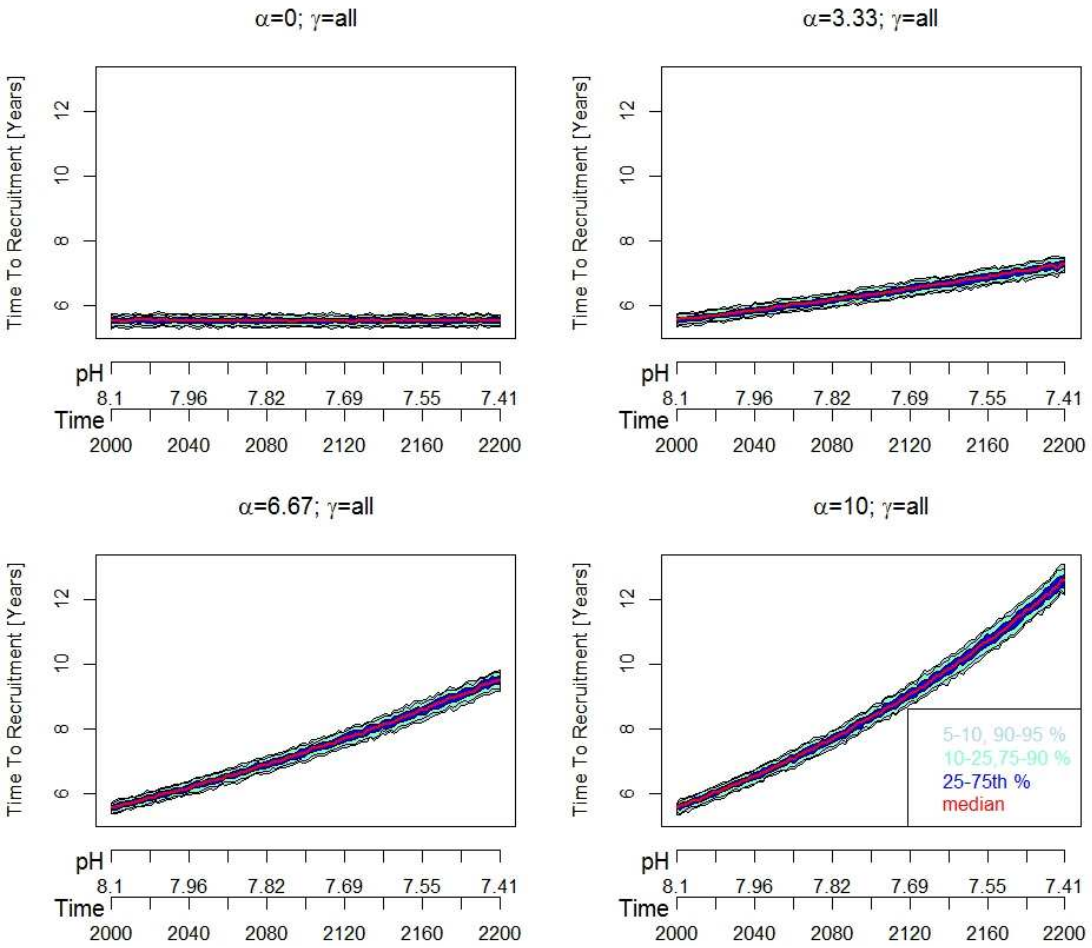

Figure 2.5. Time to recruitment for eggs spawned in each year from 2000 to 2200 from the stochastic model. Shaded areas about the time-trajectory of the median time to recruitment represent probability intervals.

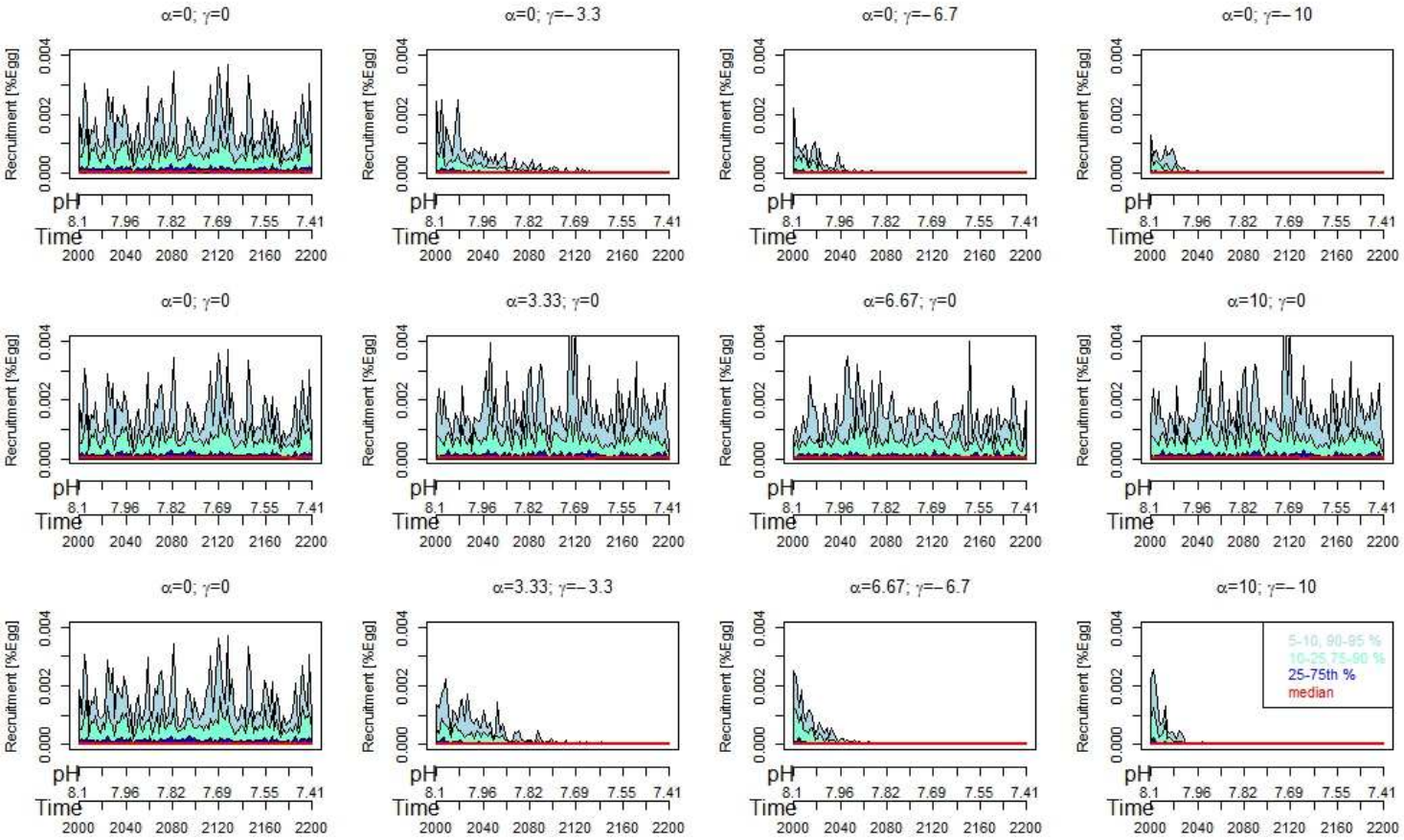

Figure 2.6. Percent of eggs spawned in each year from 2000 to 2200 which recruit from the stochastic version of the model. Shaded areas about the time-trajectory of the median percent number of eggs which survive to recruit represent probability intervals.

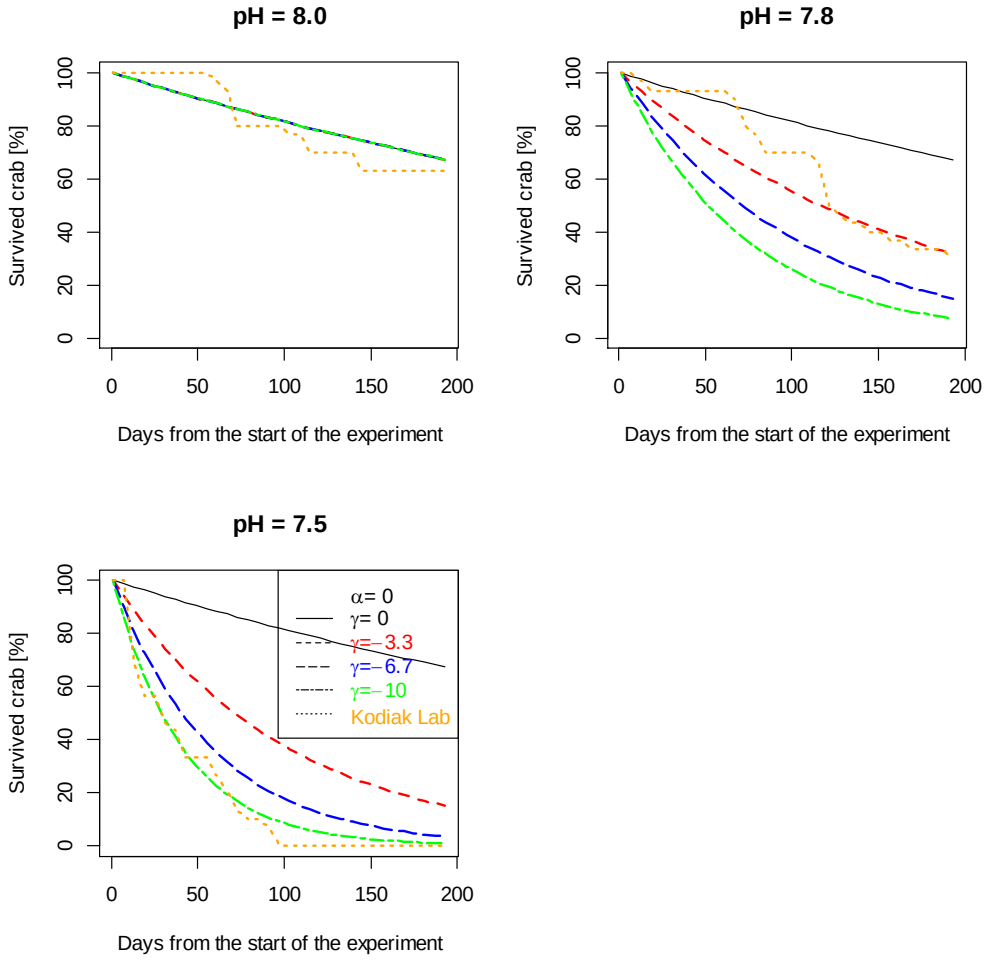

Figure 2.7. Modeled crab survival vs. survival of juvenile red king crab in the Kodiak Laboratory experiments.

Appendix 2.A: Derivation of Equations (2.3)

Let S be the survival rate for a given stage, n be the minimum number of time-steps that an animal needs to be in the stage before it can move to the next step, and p be the probability of moving to the next stage each time-step once an animal has been in the stage for n time-steps (moving to the next stage takes place at the end of the time-step after survival). For the case n=3, the dynamics of the stage can be written as:

$$\begin{pmatrix} 0 & 0 & 0 & 0 \\ S & 0 & 0 & 0 \\ 0 & S & S(1-p) & 0 \\ 0 & 0 & Sp & 1 \end{pmatrix} \begin{pmatrix} N_1 \\ N_2 \\ N_{3+} \\ \Omega \end{pmatrix} \tag{2.A.1}$$

where N_1, N_2, N_{3+} are the numbers of animals which have been in the stage for 1, 2 and 3+ time-steps, and Ω is the number of animals which have left the stage.

The number of animals leaving the stage are $S^3 p$ after 3 time-steps, $S^4(1-p)p$ after 4 time-steps, $S^5(1-p)^2 p$ after 5 time-steps, etc. This is a geometric progression of the form ($S^3 p(1+(1-p)S+(1-p)^2 S^2..)$ which sums to:

$$\frac{S^3 p}{1-(1-p)S} \tag{2/A.3}$$

Generalizing Equation 2.A.3 from a minimum of 3 to n time-steps leads to Equation 2.3.

The average time to leave a stage is:

$$\sum_{i=1} i\, N_{3+,i} S\, p \,/ \sum_i N_{3+,i} S\, p \tag{2.A.4}$$

where $N_{3+,i}$ is the number of animals in the 3+ class at the start of time-step i.

Chapter 3: Ocean acidification impact on Bristol Bay Red king crab under various harvest strategies

3.1 Introduction

3.1.1 Fishery management

The fishery for Bristol Bay red king crab is managed by the State of Alaska through a federal fishery management plan (FMP). The goal of the FMP is to maximize the overall long-term benefit of Bering Sea and Aleutian Islands (BSAI) king and Tanner crab stocks to the nation, consistent with responsible stewardship for conservation of the crab resources and their habitats (NPFMC, 2011). The FMP consists of two sets of rules, one under state and one under federal jurisdiction by the North Pacific Fishery Management Council (NPFMC). Federal rules, such as those used to set overfishing levels (OFLs), are fixed in the FMP and require an FMP amendment to change. State management rules determine legal catchable crab sizes, total allowable catch, catch season, catch areas, sex restrictions, and rules related to reporting and inspections (NPFMC, 2008). State rules are set at the federal level, but can be modified by the state based on criteria in the FMP.

The abundance of Bristol Bay red king crab is estimated using stock assessments conducted by the Alaska Department of Fish and Game (ADFG; e.g., Zheng and Siddeek, 2010). These assessments are based on a sex- and length-structured population dynamics model that uses NMFS survey data, commercial catch data, and observer data for parameter estimation. The directed (pot) fishery for red king crab is managed using a total allowable catch (TAC) which is determined according to a state harvest control rule (Table 3.1) and the Tier 3 OFL control rule (Table 3.2). The state harvest control rule is a function of current-year estimates of the biomass of mature female crabs that are estimated to successfully mate in a given year, or the effective spawning biomass (ESB), and is implemented in conjunction with restrictions on size, sex, and season. Specifically, only males with a carapace width $\geq$ 6.5-in may be harvested, and no fishing is allowed during molting and mating periods. An annual prohibited species catch (PSC) cap limits the number of Bristol Bay red king crab that can be taken by the groundfish fishery. The PSC limits are based on the previous-year ESB. Estimates of the biological reference points $B_{35\%}$ and $F_{35\%}$ are used to determine the overfishing level for Bristol Bay red king crab, which is currently classified a Tier 3 stock under the BSAI crab in FMP (NPFMC, 2008). $F_{35\%}$ is the exploitation rate at which mature male biomass-per-recruit (MMB/R) is reduced to 35% of its unfished level. MMB/R is computed using a size-transition matrix for males and the assumption that future retained and discard male selectivities will equal the average of those for 2006-2008. Average recruitment during 1995-present is used to estimate $B_{35\%}$ (the mature male biomass corresponding to $F_{35\%}$ if recruitment is set to that at which MSY is achieved). This set of years was argued by Zheng and Siddeek (2010) to reflect current (and likely) future recruitment.

In this chapter, post-recruits and ocean acidification impacts on recruitment are modeled within a simplified version of the stock assessment model for Bristol Bay red king crab. The model is projected forward for a no-ocean acidification (no-OA) (base case) scenario and scenarios in which OA impacts the population dynamics, in terms of biological (mature male biomass, catch) and economic (profit) performance metrics, under various harvest strategies.

3.2 Methods

3.2.1 Modeling post-recruits

The post-recruits (and hence the impacts of the fishery) are modeled using a population dynamics model which is a simplification of the current stock assessment model in which only males are modeled, fewer size-classes are used and no consideration is taken of shell condition. Male mature biomass (MMB) at the time of mating is used as a proxy for fertilized egg production in this model as recommended by a Center for Independent Experts (CIE) review (NMFS, 2008) owing to many uncertainties in estimating female mature biomass and the number of fertilized eggs. The basic dynamics of the population in the model are:

$$\underline{N}_{y+1} = \mathbf{X}\mathbf{S}_y\underline{N}_y + \underline{R}_{y+1} \tag{3.1}$$

where $\underline{N}_y$ is the vector of numbers-at-length (males only) at the start of year *y*, $\mathbf{X}$ is the size-transition matrix, $\mathbf{S}_y$ is the survival matrix for year *y*, and $\underline{R}_y$ is the vector of recruits for year *y*. $\mathbf{S}_y$ is a diagonal matrix with elements:

$$S_{y,i,i} = e^{-M_y}(1 - S_i^T F_y^T)(1 - S_{y,i}^D F_y^D) \tag{3.2}$$

where M_y is the instantaneous rate of natural mortality for year y, S_i^T is selectivity due to trawl fishery bycatch on animals in size-class *i*, F_y^T is the exploitation rate due to the trawl fishery during year y, $S_{y,i}^D$ is selectivity for the directed fishery during year y on animals in size class *i*, and F_y^D is the exploitation rate due to the directed fishery during year y. Bristol Bay red king crab have historically also been caught and discarded by the fishery for Eastern Bering Sea Tanner crab, but this source of mortality is ignored for the analyses of chapter as it has been very low in recent years. In model projections, F_y^T in Equation (3.2) are set to the average over 2006-2011. The retained catch (in mass) by the directed fishery during year y, C_y, is:

$$C_y = \sum_i Q_i\, w_i\, S_i^D\, F_y^D\, N_{y,i}\, e^{-\delta M_y} \tag{3.3}$$

where Q_i is the proportion of crab in size-class i which is retained, w_i is the average mass of a male crab in size-class *i*, $N_{y,i}$ are numbers of animals in size class *i* at the start of year *y*, and δ is the time from the survey to the fishery.

$$MMB_y = \sum_i N_{y,i}\, f_i\, e^{-(2/12+\delta)M_y}(1 - S_{y,i}^D F_y^D) \tag{3.4}$$

where MMB_y is the mature male biomass during year *y* at the assumed time of mating (15 February of year *y*+1), and f_i is the fecundity of a crab in size-class *i*. Initial numbers at size (N_i) are given in Table 3.3.

Recruitment only occurs to the first size-class in the model. Recruitment during year y is calculated as the sum of the numbers recruiting during year *y* based on spawning during years y', where the spawning year ranges from 1 to 10 years before year *y*.

$$R_y = \sum_{y'=y-10}^{y-1} \phi\, f(MMB_{y'})\, G(y', y) \tag{3.5}$$

where $G(y', y)$ is the fraction of animals which were spawned during year *y'* which recruit during year *y*. The function G sums the recruited animals for the given spawn year, which were projected forward using the pre-recruit population model (Equations 2.1 and 2.2). The symbol ϕ is a constant, computed so that the population is stable in the absence of OA $(\gamma = 0)$, and exploitation $(F_y^D = F_y^T = 0)$. To find the value of this parameter, R_y is set to 1, the resulting MMB is found, and $G(y', y)$ is set based on the pre-recruitment model with no OA impact, i.e.:

$$\phi = 1 / \sum_{y'=y-10}^{y-1} f(MMB_{y'})\, G(y', y) \tag{3.6}$$

where recruitment is governed by a Ricker stock-recruitment relationship, i.e.:

$$f(MMB_{y'}) = R_0 \frac{MMB_{y'}}{MMB_0} e^{\frac{5}{4}\ln(5h)\left(1-\frac{MMB_{y'}}{MMB_0}\right)} \tag{3.7}$$

and $MMB_{y'}$ can be a historical or projected value. The steepness of the stock- recruitment relationship is *h*, and R_0 and MMB_0 are respectively the recruitment and mature male biomass in an unfished state.

A list of the pre-specified model parameters is given in Table 3.3.

3.2.2 Projections

3.2.2.1 Constant F projections

The model is projected forward under five constant exploitation rates for the directed fishery, F^D (0, 0.11, 0.18, $F_{35\%}$ (=0.22), and 0.25) for each γ, where γ is set to 0 in the no-OA scenario, and to -3.33, -6.66, and -10 in the OA scenarios.

3.2.2.2 Control rule projections

The model is projected forward for each OA scenario with F_y^D based on the NPFMC OFL control rule (Table 3.2). Only the OFL control rule is used in the projections, because the State harvest rule is always more conservative than the federal OFL control rule. Hence, projections based on the OFL control rule are sufficient to show the most extreme consequences of OA on the population of red king crab in Bristol Bay given state management decision making.

3.2.2.3 Optimal fishery and economic projections for constant and time varying exploitation rates

The time-series of values for F_y^D are found for each OA scenario that maximize total catch (Equation 3.3) and the present value of discounted profits using a non-linear search technique that maximizes objective functions described by Equations 3.10a-c.The maximization is based on estimating a separate value of F_y^D for each future year rather than applying a control rule, although Equations 3.10a and 3.10b include a penalty (O_y) (Equation 3.11) to avoid large changes in exploitation rate (the restriction level (rl) on year-to-year changes in exploitation rate is set to 0.01 for these calculations; Equation 3.11). The resulting values for MMB and F_y^D are, however, plotted against each other to identify a possible harvest control rule.

Discounted profit (π_y) is calculated for three levels of cost V_y (minimum, median, and maximum; Equation 3.9) and is defined as:

$$\pi_y = (\beta)^{(y-y_0)}(p_y C_y - V_y) \tag{3.8}$$

where β is a discount factor (Table 3.3), p_y is price per kg during year y (Table 3.3), y_0 is the first year of the projection period (2000), and V_y is the variable cost during the year y, calculated for the costs of fuel, food, and bait:

$$V_y = E_y c_F + E_y c_G + 488624 F_y^D c_b \tag{3.9}$$

where E_y is a sum of days fishing (E_y^F) and days traveling (E_y^T), and c_F, c_G and c_b are respectively the average daily costs of fuel and food, and bait cost per potlift (Table 3.3). The number of potlifts is calculated as a linear function of days fishing, Potlifts=$78.334\,E_y^F$ (Figure 3.1), while days fishing are calculated as a linear function of F_y^D, $E_y^F = 6237.7\,F_y^D$ (Figure 3.2), and days traveling as a linear function of days fishing, $E_y^T = 0.5021\,E_y^F$ (Figure 3.3), where a combination of the three results Equation 3.9.

The three objective functions: (a) maximize the total catch subject to a penalty on changes over time in exploitation rate due to the directed fishery (Equation 3.10a), (b) maximize the total discounted profit subject to a penalty on changes over time in exploitation rate due to the directed fishery (Equation 3.10b), and (c) maximize the total catch given linear and quadratic parameters *a* and *b* in the quadratic function (Equation 3.10c). The quadratic function represents an abstract form of discounted profits. For example, parameter *a* on the linear term could represents net benefits in the form of ex-vessel price minus the linear costs in equation (3.9), and the quadratic parameter *b* can be interpreted as a non-linear cost that implies decreasing returns to scale.

$$\sum_y (C_y - \lambda_1 O_y) \tag{3.10a}$$

$$\sum_{y}(\pi_y - \lambda_2 \mathrm{O}_y) \tag{3.10b}$$

$$\sum_{y}(\beta)^{(y-y_0)}(a\sum_{i} C_y - b\sum_{i}(C_y)^2) \tag{3.10c}$$

where the values for $\lambda_{1,2}$ are set to scale the penalty to the size of the catch (Equation 3.10a) and the profit (Equation 3.10b). The penalty, O_y, is defined as:

$$\mathrm{O}_y = \begin{cases} \left([F_y^D - F_{y-1}^D]/F_{y-1}^D\right)^2 & \text{if } \left|(F_y^D - F_{y-1}^D)/F_{y-1}^D\right| > rl \\ 0 & \text{otherwise} \end{cases} \tag{3.11}$$

where *rl* is the restriction level on year-to-year changes in exploitation rate, set to 0.01.

3.2.2.3.1 Parameterization of the objective functions

The values for the parameters to scale the penalties, λ_1 and λ_2, are chosen such that i) the projected exploitation rates, MMB and catch in Equations 3.10a and 3.10b best match their values for an exploitation rate of $F_{35\%}$ for the no-OA scenario, ii) the exploitation rate is zero before the end of the projection period for all OA scenarios, and iii) the time-series of exploitation rates are relatively stable. The chosen values for λ_1 and λ_2 are related to the absolute magnitude of the catch and profit in Equations 3.10a (tonnes) and 3.10b ($mil). λ_1 is set to $100C_{F_{35\%}}$, where $C_{F_{35\%}}$ is the equilibrium catch when $F_y^D = F_{35\%}$, and λ_2 is set to 4.

The same criteria used to set λ_1 and λ_2 were used to set a and b in Equation 3.10c. In addition, the exploitation rate by the directed fishery equals zero when a = 0 and this condition implied a value for b of $1/C_{F_{35\%}}$. Solving for the optimal constant exploitation rate that corresponds to each positive value of a indicated a spike in optimal exploitation rate at approximately $a = 1.5$ (Figure 3.4a). This was due to the impact of the initial size-structure of the population. Projections in which the summation in Equation 3.10c was restricted to projection years 2011-2099 showed no such spike (Figure 3.4b). The parameter a was set to 4 for the analyses reported here.

3.2.3 Implementation in the R statistical package

Figure 3.5 outlines the structure of the code that was used to implement the analyses of this chapter. There are two main parts to the code, those which implement (a) the population dynamics model and (b) the objective function. The code for the population model contains sub-routines that calculate population numbers-at-length (Equation 3.1) in response to exploitation rate, and the impact of ocean acidification on recruitment (Equation 3.5). It also contains the routines to read in the input data and the values for the numbers-at-length at the start of the projection period.

The R optimization tool, *optim*, is called with initial values for the parameters (F_y^D), which are passed from the code for the objective function to the code for the population model. The

code for the population model returns the penalty, the time-series of catches, and discounted profit (Equations 3.11, 3.3 and 3.8, respectively) to the code implementing the objective function, which is then minimized according to a specified objective function (Equations 3.10a-c).

3.3 Results

The results are summarized by plots of 100-year time-trajectories of catch, exploitation rate, MMB, and profit, and by tables of total catch and MMB over the 100-year projection period, average discounted profit over the 100-year period, and the years in which catch, discounted profit and MMB which first drop to 5% of the equilibrium values when the exploitation rate is $F_{35\%}$ for the no-OA scenario (Table 3.4; rows "F^D=0.22"). The x-axes for each plot indicate both year and the pH projected for the year concerned.

3.3.1 Constant F and $F_{35\%}$ projections

The catch and biomass equilibrate at non-zero values for the no-OA scenario and are driven to zero at all exploitation rates in the OA scenarios (Figures 3.6 and 3.7). Catch and MMB increase initially owing to the initial numbers-at-length.

MMB first drops to 5% of the B_{MSY} under a constant exploitation of $F_{35\%}$ when there is no OA impact in 2050, 2036, 2030 for respectively for the γ = -3.33, -6.67, and -10 scenarios (Table 3.4c; row "F^D=0.22"). As expected, catch and biomass reach the threshold at essentially the same time, but because of costs, profit drops to 5% of that corresponding to $F_{35\%}$ 3-5 years earlier (Table 3.4c; row "F^D=0.22").

Lower exploitation rates lead to a longer time before the biomass thresholds are breached (Table 3.4c), but the longer times do not necessarily lead to higher profits. Total discounted profit is highest for the three OA scenarios when F=0.25yr^{-1} (Table 3.4a,b; rows "F^D=0.25").

3.3.2 Harvest control rule projections

Projected MMB and catch drop to 5% of the equilibrium values under an exploitation of $F_{35\%}$ under the no-OA scenario, and in the OA scenarios when the annual exploitation rate is based on the OFL control rule in 2073, 2049, 2041 and 2049, 2033, and 2027, respectively (Table 3.5c). The catch and discounted profit drop below the threshold before the MMB for the OA scenarios because the OFL control rule requires fishery closure at low stock biomass (Figure 3.8). The OFL control rule performs better than the constant exploitation rate strategies in terms of conserving the resource, because it closes the fishery at low biomass levels, which are also unprofitable and which happen sooner for the more extreme OA scenarios (Figures 3.6-3.8; Tables 3.4a,b and 3.5a,b). Discounted profits for the OFL control rule are 19.5, 13.2, 11.2, and 10.2 ($mil) for the four OA scenarios (Table 3.5a), which are very close to projected profits for the $F_{35\%}$ strategy (19.9, 13.1, 11.3, and 10.4 ($mil)) and higher than those for the F^{D}=0.11 and 0.18 strategies (Tables 3.4a,b, 3.5a,b).

3.3.3 Selecting exploitation rates to maximize Equation 3.10a and b

Figure 3.9 shows the sensitivity of the results to λ_2 when the time-series of exploitation rates for the directed fishery are selected to maximize discounted profit (Equation 3.10b) when the values for the cost parameters are set to their median values (Table 3.3) and the discount rate is set to $\beta = 0.95$. Low values for λ_2 lead to projected exploitation rates that oscillate unrealistically, while exploitation rates do not drop to zero at high levels of λ_2 for the γ = -3.33 and -6.6 scenarios. The time-trajectory of exploitation rates is relatively stable and converge to zero in the γ = -6.67 and γ = -10 scenarios when λ_2 is set to 4. The parameter λ_1 is set to $100C_{35\%}$.

The present value of discounted profits for the strategies which maximize catch and profits in Eq. 3.10a and 3.10b (Figures 3.10 and 3.11) differ by less than 1% for the γ=0 scenario (19.7 vs. 20.1 ($mil)) (Tables 3.6a,b, and 3.7a,b; "F_y^D (β=0.95)"). The strategy that maximizes Equation 3.10b leads to discounted profits that are 3-5% greater than the strategy which maximizes catch in Equation 3.10a for the three OA scenarios. The strategy which maximizes profits depletes the stock below the biomass threshold 2-8 years later than the strategy which maximizes catch (Tables 3.6c, and 3.7c; row "F_y^D (β=0.95)"). However, the average MMB over the projection period for the strategy which maximizes profits in Equation 3.10b is 22%, 27%, 15% and 14% lower than the strategy which maximizes catch for the four scenarios. Maximizing profits reduces MMB to the biomass threshold in 2055, 2036, and 2031 under the three OA scenarios, 2-4 years sooner than the strategy that maximizes catch (Table 3.6c, 3.7c). Catches are the same for no-OA scenario and higher by 3%, 2%, and 2% for the three OA scenarios for the strategy which maximizes catch than in the strategy which maximizes profit, as expected. The latter strategy reduces catches below 5% of that under the constant $F_{35\%}$ strategy 1-4 years sooner than the former strategy (Tables 3.6b,c, and 3.7b,c; rows "F_y^D (β=0.95)").

Higher discount factors lead to higher biomasses and catches (Table 3.7a; Figure 3.12). Fishery costs are another factor which determine profits. The fishery is closed earlier for higher costs (food, fuel, and bait costs) for the OA scenarios (Figure 3.13; Table 3.3) when the exploitation rates are selected to maximize profit. This is expected because higher costs lead to lower profits. Moreover, and as expected, the scenario with the lowest costs leads to the highest discounted profits (Table 3.7a,b).

The first 10 years of the time-series of MMB and exploitation rate are omitted from Figure 3.14, because they appear unstable owing to the influence of the initial years (0-10) on the exploitation rates that maximize the objective function in Equation 3.10b. The estimated MMB and exploitation rates are simultaneously decreasing over time for all OA scenarios, and the opposite is the case for the no-OA scenario. The stronger the OA impact is, the more abruptly exploitation rate decreases to zero.

3.3.4 Selecting exploitation rates to maximize Equation 3.10c

Equation 3.10c is maximized under the constant exploitation rate of 0.265 for the no-OA scenario when catch in all years is included in objective function, and is maximized at a lower rate (0.216) when the first 11 years of catch are ignored when computing the objective function

(Figures 3.15a, 3.15b, respectively, and Table 3.9a,b; rows "F^D (β=0.95)" and F^D_{11-99}(β=0.95)"). The latter exploitation rate is closer to the value of F_{MSY} (0.222).

Time trajectories of exploitation rate that are allowed to vary annually when maximizing Equation 3.10c, projected MMB, catch and discounted profit (Figure 3.16) are within 1% of the values when the future exploitation rate is assumed to be constant in Figure 3.17 (Table 3.8a,b; rows "F^D (β=0.95)" and "F^D_y (β=0.95)"). Exploitation rates and discounted profits for the three discount factors when exploitation rate is allowed to vary annually (Figure 3.18) are within 1% of the profits for the constant exploitation rates in Figure 3.15a (Table 3.8a,b; F^D rows compared with F^D_y rows for the same β values).

3.4 Discussion

The OFL control rule achieves higher discounted profits than the constant exploitation rate (F^D = 0.11, 0.18, and 0.22) strategies, while the catch is 25% higher and MMB is 55% lower than that for the lowest exploitation rate considered (0.11) at γ=0. The OFL control rule achieves this by closing the fishery once the biomass is reduced below the cut-off value and hence it avoids negative profits. In contrast, the constant exploitation rate strategies do not respond to biomass and so negative profits are possible.

Estimated exploitation rates and discounted profits at three levels of the discount factor β are larger for smaller values of γ when profit and catch are maximized, except in the scenarios where β=0.99 and γ = -3.33, where exploitation rate is estimated lower than for γ =0 (Table 3.9). This apparent inconsistency agrees with the MMB trajectories for the same scenarios for β=0.99 at γ=-3.33 and γ=0 in Figure 3.19, where MMB is estimated larger at γ =-3.33 than at γ =0 at about the 15th year of the projection period. This apparent inconsistency is due to the influence of the initial years on exploitation rates in the objective function (Figure 3.15b and Table 3.9).

Harvest strategies in which the exploitation rate was time-invariant allowed for the stock to fall below minimum stock size threshold (MSST=1/2 B_{MSY}), i.e., to become overfished (Zheng and Siddeek, 2010) although how to define MSST in the face of changing environment is unclear.

Higher harvesting costs (fuel, food, and bait) reduce discounted profits. Exploitation rates and profits decrease with an increase in variable harvest costs when profit is maximized (Figure 3.13).

The analyses of this chapter assume no changes to the growth rate or (non-fishery) survival of post-recruit red king crab in response to OA. The parameters of the Ricker stock-recruitment relationship are also assumed constant for the OA scenarios. It is not clear whether these parameters would change due to OA impacts (NOAA Ocean Acidification Steering Committee, 2010). However the stock-recruitment relationship could become less productive given unfavorable environmental conditions under OA. The natural mortality rate in the simplified version of the population dynamics model (Zheng and Siddeek, 2010) used for this analyses is also assumed to be time-invariant, but it may increase, which would be consistent with the trend towards higher mortality rates under OA for larvae and juveniles measured in the Kodiak Laboratory research (Long et al., in press). An increase in the natural mortality rate for red king crab would contribute to the negative OA impact on red king crab MMB. Potential

changes in the stock-recruitment relationship and the natural mortality rate for post-recruits would compound the effects of OA modeled here.

Finally, prices and costs are likely to change over the next 100 years whereas they are assumed to be constant for the analyses of this chapter. The exploitation rates which maximize discounted profit (Equation 3.10b) would be higher as would discounted profits if prices increased over time, but costs remained constant, and *vice versa*.

3.5 References

National Marine Fishery Service (NMFS). 2008. Final Environmental Assessment for Amendment 24 to the Fishery Management Plan for Bering Sea/Aleutian Islands King and Tanner Crabs to Revise Overfishing Definitions. Prepared by staff of the Alaska Fisheries Science Center: Seattle and Kodiak, Alaska Department of Fish and Game, National Marine Fishery Service, Alaska Region, and North Pacific Fishery Management Council. National Marine Fisheries Service, P.O. Box 21668, Juneau, AK 99802-1668.

Long W.C., Swiney, K.M., Harris, C., Page, H.N., and Foy, R.J. 2013. Effects of ocean acidification on juvenile red king crab (*Paralithodes camtschaticus*) and Tanner crab (*Chionoecetes bairdi*). Kodiak Laboratory, Resource Assessment and Conservation Engineering Division, Alaska. FSC, NMFS, NOAA. (in press)

NOAA Ocean Acidification Steering Committee. 2010. NOAA Ocean and Great Lakes Acidification Research Plan, NOAA Special Report, 143 pp.

North Pacific Fishery Management Council (NPFMC). 2008. Amendment 24. Final Environmental Assessment for amendment 24 to the Fishery Management Plan for Bering Sea/Aleutian Islands King and Tanner Crabs to Revise Overfishing Definitions.

North Pacific Fishery Management Council (NPFMC). 2011. Fisheries Management Plan for the King and Tanner Crab Fisheries of the Bering Sea and Aleutian Islands. North Pacific Fishery Management Council. Anchorage.

Zheng, J., and Kruse, G.H. 2003. Stock-recruitment relationships for three major Alaskan crab stocks. Fish. Res. 65: 103–121.

Zheng, J. and Siddeek, M.S.M. 2010. Bristol Bay red king crab stock assessment in fall 2010. In: 2010. Stock Assessment and Fishery Evaluation Report for the King and Tanner Crab Fisheries of the Bering Sea and Aleutian Islands Region: 2010 Crab SAFE. North Pacific Fishery Management Council, Anchorage.

3.4 Figures and Tables

Table 3.1. State harvest strategy specifications for BSAI Bristol Bay red king crab.

Stock threshold for opening fishery:
8.4 million mature females, and 14.5 million pounds of effective spawning biomass (ESB)
Exploitation rate on mature-sized (≥120 mm CL) male abundance:
10%, when ESB <34.75 million pounds
12.5%, when ESB is between 34.75 million pounds and 55.0 million pounds
15%, when ESB ≥55.0 million pounds
Harvest capped at 50% of legal male abundance:
Minimum TAC:
4.444 million pounds (including portion allocated to CDQ fishery)

Table 3.2. Specification of the exploitation rate used to compute the OFL for Tier 3 stocks. *B* is a measure of current reproductive capacity (MMB for Bristol Bay red king crab); $B^*=B_{35\%}$, a proxy for B_{MSY}, which is the biomass at which MSY is achieved; $F^*=F_{35\%}$, the exploitation rate which reduces mature male biomass biomass-per-recruit to 35% of its unfished level; and $0\leq\alpha\leq\beta$ and $0\leq\beta\leq1$ are restriction parameters, with default values of 0.1 and 0.25, respectively.

$\frac{B}{B^*} > 1$	$F_{OFL} = F^*$
$\beta < \frac{B}{B^*} \leq 1$	$F_{OFL} = F(\frac{B/B^* - \alpha}{1-\alpha})$
$\frac{B}{B^*} \leq \beta$	Directed fishery $F = 0$ and $F_{OFL} \leq F^*$

Table 3.3 Model parameters fixed in the base-case (no-OA) model, and the initial numbers-at-length.

Parameter	Size-class (mm)				
	65-80	**80-100**	**100-120**	**120-140**	**140+**
Weight per class, w_i [kg]	0.324714	0.652966	1.180429	1.946525	3.064985
Fecundity, f_i	0	0	0	1.946525	3.064985
Size-transition matrix, X	3.80E-05	0.99996	0	0	0
	0	0.32988	0.67012	0	0
	0	0	0.156486	0.843514	0
	0	0	0	0.549888	0.450112
	0	0	0	0	1
Retained fraction per class, Q_i	0	1.30E-6	0.002179	0.516693	0.999167
Selec. groundfishery, S_i^T	3.17E-02	0.060261	0.235422	0.531515	0.99
Selec. pot fishery, S_i^D	1.0E-20	0.060246	0.254154	0.658982	0.99
Initial numbers, N_i	11170.30	10117.90	6099.39	11285.20	12677.60

Parameter	Value
Unfished recruitment, R_0	17282.5
Steepness, h	0.859317
$F_{35\%}$	0.221697
F^T	0.00481205
δ	0.5
Natural mortality, M [yr^{-1}]	0.18
Price per kg, p_y [$/kg]	11.00295
Discount factor, β	0.95

Years	2006	2007	2008	2009	2010
F^D	0.221606	0.282729	0.280152	0.196708	0.164573
Days Fishing (E_y^F)	1096	1489.5	1779.5	1414.75	1604
Potlifts	72218	112626	139329	117782	132661
Days Traveling (E_y^T)	714.5	849	776.5	724	717

Potlifts = 78.334(E_y^F)	R^2=0.89
E_y^F =6237.7 F_y^D	R^2=-1.05
E_y^T =0.5021 E_y^F	R^2=-3.41

	median	min	max
Fuel cost per day, c_F [$/day]	3209.5	882.0	5953.5
Food cost per day, c_G [$/day]	305.6	11.0	771.8
Bait cost per day, c_b [$/day]	15.8	4.4	28.7

Table 3.4 (a) Average catch, MMB, and discounted profit based on 100-year time trajectories under constant exploitation rates, (b) percentage change in the average catch, MMB, and profit relative to the values when exploitation rate is $F_{35\%}$ (0.22), and (c) years in which catch, MMB and profit first drop to 5% of the equilibrium values when exploitation rate is $F_{35\%}$ for the no-OA scenario.

	Total catch ('000t)				Average MMB ('000t)				Discounted profit ($mil)			
	γ=0	γ=-3.33	γ=-6.67	γ=-10	γ= 0	γ=-3.33	γ=-6.67	γ=-10	γ= 0	γ=-3.33	γ=-6.67	γ=-10
F^D=0.11	8.3	2.3	1.6	1.4	85.0	23.2	16.1	13.5	18.9	10.1	8.6	7.8
F^D=0.18	10.5	2.7	1.9	1.7	64.3	16.1	11.5	9.8	19.8	12.5	10.7	9.8
F^D=0.22	10.9	2.7	2.0	1.7	53.4	13.1	9.5	8.2	19.9	13.1	11.3	10.4
F^D=0.25	10.8	2.7	2.0	1.8	46.4	11.3	8.4	7.3	19.9	13.2	11.4	10.6
F^D=0.11	76.5	84.6	80.3	78.5	159.3	177.6	169.1	165.4	94.8	77.4	76.2	75.5
F^D=0.18	96.6	98.8	96.5	95.5	120.6	123.7	121.0	119.8	99.3	95.6	94.9	94.5
F^D=0.22	100.0	100.0	100.0	100.0	100.0	100.0	100.0	100.0	100.0	100.0	100.0	100.0
F^D=0.25	99.1	99.0	100.7	101.5	87.0	86.7	88.1	88.8	100.0	101.1	101.7	102.0
F^D=0.11	-	2056	2039	2032	-	2062	2043	2035	-	2052	2036	2030
F^D=0.18	-	2053	2038	2031	-	2054	2038	2032	-	2048	2034	2028
F^D=0.22	-	2051	2036	2031	-	2050	2036	2030	-	2045	2032	2027
F^D=0.25	-	2049	2036	2030	-	2048	2034	2029	-	2043	2031	2026

Table 3.5(a) Average catch, MMB, and discounted profit based on 100-year time trajectories under the OFL rule, (b) percentage change in the average catch, MMB, and profit relative to the values when the exploitation rate is $F_{35\%}$ (Table 3.4a; row "F^D=0.22"), and (c) years in which catch, MMB and profit first drop to 5% of the equilibrium values when the exploitation rate is $F_{35\%}$ for the no-OA scenario.

	Total catch ('000t)				Average MMB ('000t)				Discounted profit ($mil)			
	γ=0	γ=-3.33	γ=-6.67	γ=-10	γ= 0	γ=-3.33	γ=-6.67	γ=-10	γ= 0	γ=-3.33	γ=-6.67	γ=-10
	10.9	2.4	1.7	1.5	54.8	19.6	13.6	11.4	19.5	13.2	11.2	10.2
	100.5	89.1	85.7	84.6	102.8	150.3	142.3	138.8	97.8	101.0	99.3	98.7
	-	2049	2033	2027	-	2073	2049	2041	-	2049	2033	2027

Table 3.6(a) Average catch, MMB, and discounted profit based on 100-year time trajectories when the time series of exploitation rates is selected to maximize the objective function in Equitation 3.10a, (b) percentage change in the average catch, MMB, and discounted profit relative to the values when the exploitation rate is $F_{35\%}$ (Table 3.4a; row "$F^D = 0.22$"), and (c) years in which catch, MMB and discounted profit first drop to 5% of the equilibrium values when the exploitation rate is $F_{35\%}$ for the no-OA scenario.

	Total catch ('000t)				Average MMB ('000t)				Discounted profit ($mil)			
	γ=0	γ=-3.33	γ=-6.67	γ=-10	γ= 0	γ=-3.33	γ=-6.67	γ=-10	γ= 0	γ=-3.33	γ=-6.67	γ=-10
a	10.9	2.7	2.0	1.8	52.8	13.7	8.3	6.4	19.7	13.0	11.5	10.7
b	100.7	100.2	100.9	102.3	99.0	104.9	86.8	78.1	99.2	99.3	101.8	103.1
c	-	2051	2035	2029	-	2051	2034	2027	-	2033	2026	2022

Table 3.7(a) Average catch, MMB, and discounted profit based on 100-year time trajectories when the time series of exploitation rates (F_y^D) is selected to maximize the objective function in Equitation 3.10b, (b) row " F_y^D (β=0.95)" is percentage change in the average catch, MMB, and discounted profit relative to the values when exploitation rate is $F_{35\%}$ (Table 3.4a; row " F^D =0.22"), whereas rows " F_y^D (Min cost; β=0.95)" and " F_y^D (Max cost, β=0.95)" are percent change with respect to the row " F_y^D (β=0.95)", (c) years in which catch, MMB and discounted profit first drop to 5% of the equilibrium values when the exploitation rate is $F_{35\%}$ (Table 3.4a; row " F^D =0.22") for the no-OA scenario.

		Total catch ('000t)				Average MMB ('000t)				Discounted profit ($mil)			
		γ=0	γ=-3.33	γ=-6.67	γ=-10	γ= 0	γ=-3.33	γ=-6.67	γ=-10	γ= 0	γ=-3.33	γ=-6.67	γ=-10
a	F_y^D (β=0.90)	9.2	2.3	1.8	1.7	29.6	6.0	4.3	3.5	10.1	9.1	8.7	8.6
	F_y^D (β=0.95)	10.9	2.6	2.0	1.7	43.4	10.8	7.2	5.6	20.1	13.4	11.9	11.2
	F_y^D (β=0.99)	11.4	2.7	2.0	1.8	52.7	14.5	9.2	7.2	72.1	22.6	17.5	15.6
	F_y^D (Min cost, β=0.95)	10.8	2.6	2.0	1.7	40.7	8.7	5.7	4.5	21.2	14.6	13.1	12.4
	F_y^D (Max cost, β=0.95)	11.0	2.6	2.0	1.7	46.4	13.0	8.5	6.7	18.8	12.2	10.6	10.0
b	F_y^D (β=0.95)	100.3	96.9	99.0	100.6	81.3	82.7	75.2	68.7	100.8	102.8	105.5	108.3
	F_y^D (Min cost, β=0.95)	98.7	98.3	99.9	100.2	93.9	80.4	79.6	80.4	105.7	108.9	110.4	110.5
	F_y^D (Max cost, β=0.95)	101.0	99.7	98.6	99.3	106.9	120.3	118.8	118.3	93.5	90.6	89.7	89.2
c	F_y^D (β=0.95)	-	2047	2034	2025	-	2055	2036	2031	-	2041	2030	2024

Table 3.8 (a) average catch, MMB, and discounted profit based on 100-year time trajectories when constant exploitation rates (F^D) and annual exploitation rates (F_y^D) are selected to maximize the objective function in Equitation 3.10c, (b) percentage change in the average catch, MMB, and discounted profit relative to the values when the exploitation rate is $F_{35\%}$ (Table 3.4a; row "F^D=0.22"), (c) years in which catch, MMB and profit first drop to 5% of the equilibrium values for $F_{35\%}$ (Table 3.4a; row "F^D=0.22") for the no-OA scenario.

		Total catch ('000t)				Average MMB ('000t)				Discounted profit ($mil)			
		γ=0	γ=-3.33	γ=-6.67	γ=-10	γ= 0	γ=-3.33	γ=-6.67	γ=-10	γ= 0	γ=-3.33	γ=-6.67	γ=-10
a	F^D (β=0.90)	8.8	2.4	1.9	1.7	26.9	6.6	4.9	4.2	9.6	8.7	8.3	8.1
	F^D (β=0.95)	10.6	2.6	2.0	1.8	42.8	9.8	6.6	5.4	19.8	13.2	11.5	10.6
	F^D (β=0.99)	10.9	2.7	2.0	1.8	51.1	13.5	8.5	6.8	69.9	21.1	14.9	12.4
	F_y^D (β=0.90)	8.7	2.4	1.9	1.7	26.3	6.5	4.9	4.2	9.6	8.7	8.3	8.0
	F_y^D (β=0.95)	10.6	2.7	2.0	1.8	42.4	9.9	6.7	5.4	19.9	13.2	11.5	10.6
	F_y^D (β=0.99)	10.9	2.7	2.0	1.8	51.2	13.5	8.6	6.8	70.2	21.0	14.9	12.4
b	F^D (β=0.95)	97.6	97.0	99.6	101.4	80.2	75.3	69.4	66.3	99.7	101.0	102.0	102.8
	F_y^D (β=0.95)	97.6	97.3	99.8	101.7	79.5	75.7	69.9	66.5	99.8	101.0	102.1	102.8
c	F^D (β=0.95)	-	2048	2034	2028	-	2045	2031	2026	-	2041	2029	2024
	F_y^D (β=0.95)	-	2048	2034	2028	-	2045	2031	2026	-	2041	2029	2024

Table 3.9 (a) constant exploitation rates (F^D) that maximize Equation 3.10c for three values of the discount factor (β), and (b) constant exploitation rates (F^D_{11-99}) that maximize Equation 3.10c for three values of (β) when first 10 years in objective function (Equation 3.10c) are ignored.

		γ= 0	γ =-3	γ =-6	γ =-10
a	F^D (β=0.90)	0.3411	0.3609	0.3768	0.3871
	F^D (β=0.95)	0.2654	0.2782	0.3051	0.3223
	F^D (β=0.99)	0.2309	0.2155	0.2471	0.2676
b	F^D_{11-99} (β=0.90)	0.2151	0.1921	0.1818	0.1725
	F^D_{11-99} (β=0.95)	0.2158	0.1807	0.173	0.165
	F^D_{11-99} (β=0.99)	0.2183	0.1652	0.163	0.157

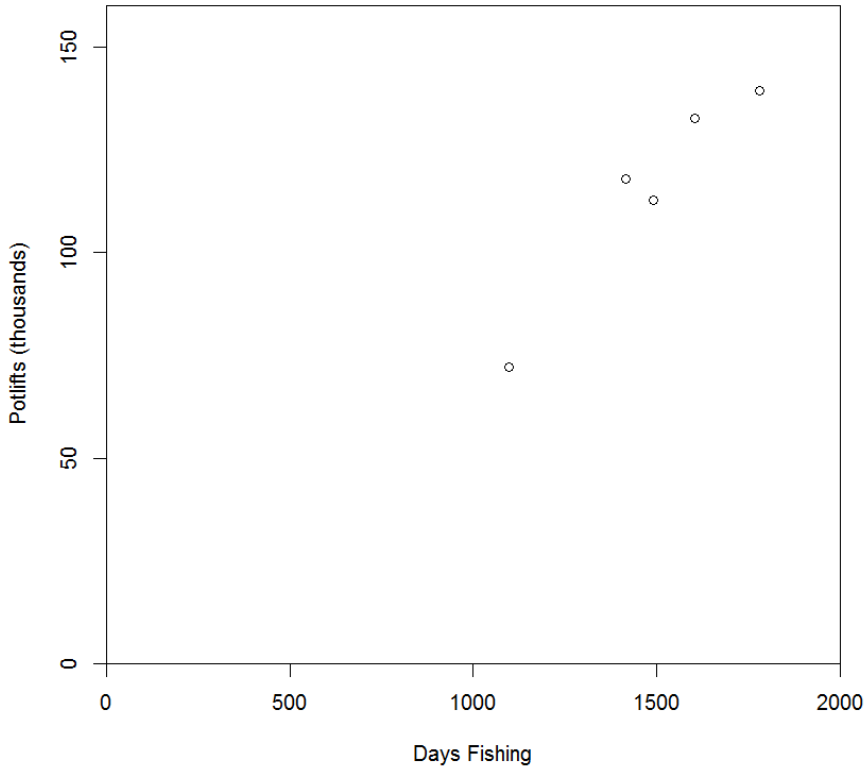

Figure 3.1. Data used in linear regression of potlifts (from the Fish Ticket database) on days fishing (from EDR data base).

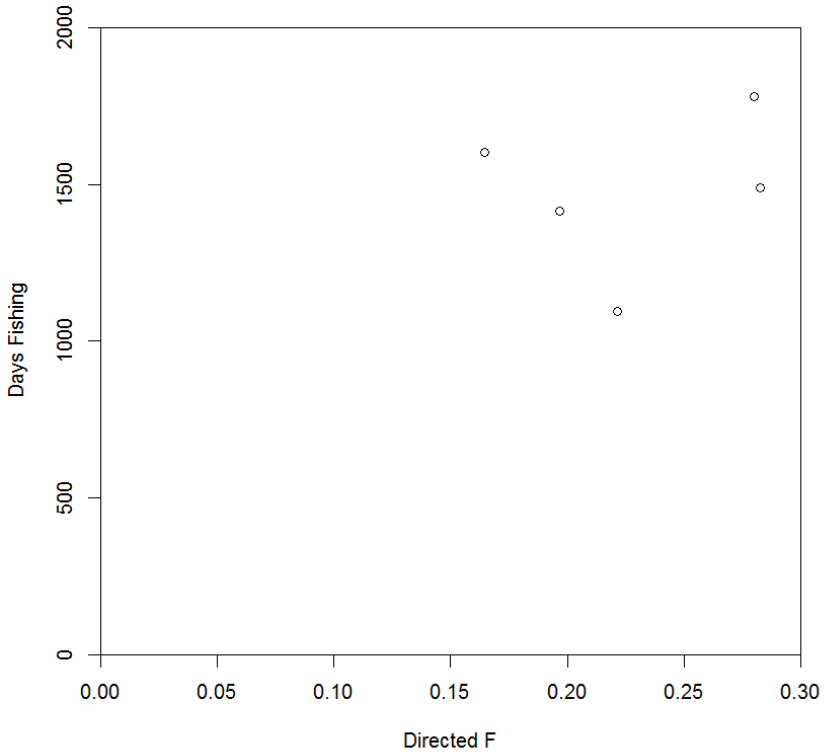

Figure 3.2. Data used in linear regression of days fishing (from the EDR data base) on the exploitation rate for the target fishery.

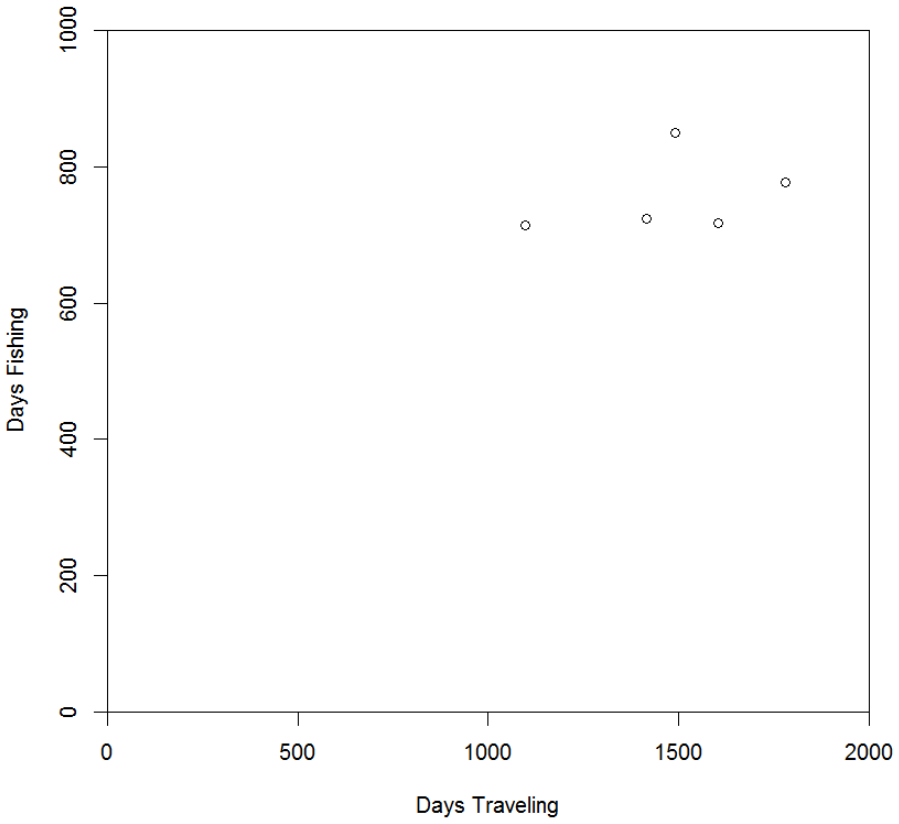

Figure 3.3. Data used in linear regression of days traveling (from the EDR data base) on days fishing (from the EDR data base).

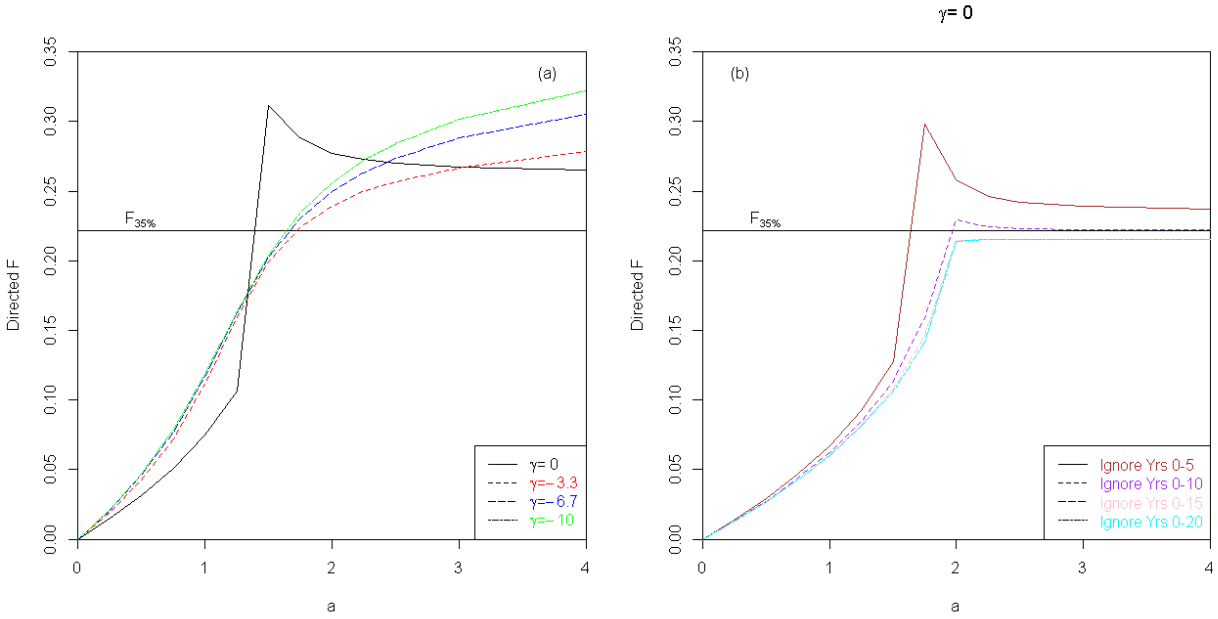

Figure 3.4. The constant exploitation rate which maximizes Equation 3.10c against the value for the parameter *a* for different values for γ (a), and the constant exploitation rate which maximizes Equation 3.10c against the value for the parameter *a* when γ=0 for different years included in the summation in Equation 3.10c (b).

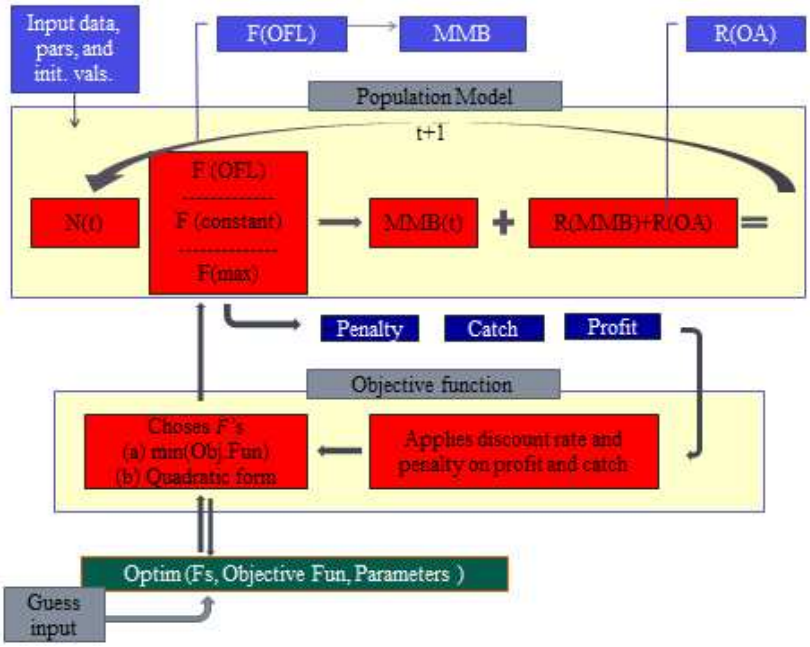

Figure 3.5. Flow chart of the code.

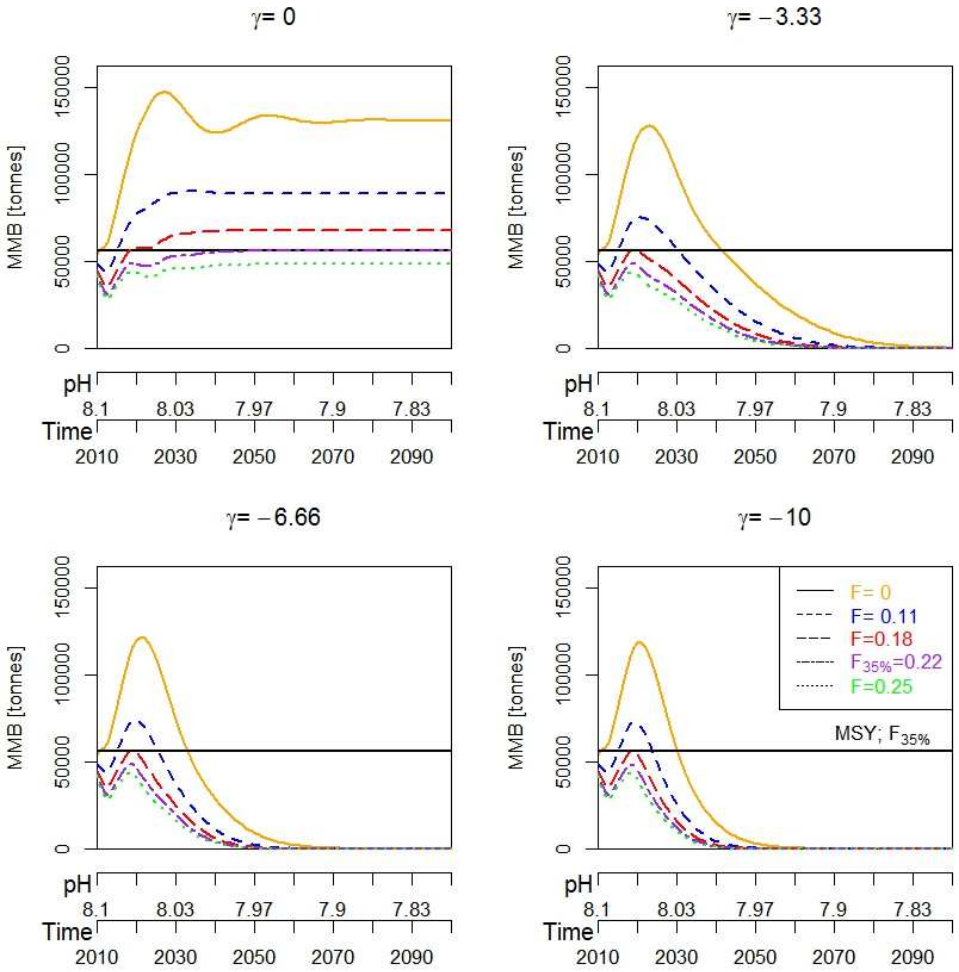

Figure 3.6. Mature male biomass of Bristol Bay red king crab under different OA (γ) scenarios for five constant exploitation rates for the directed fishery. The horizontal line denotes the equilibrium mature male biomass when the exploitation rate equals F35% and there is no OA impact.

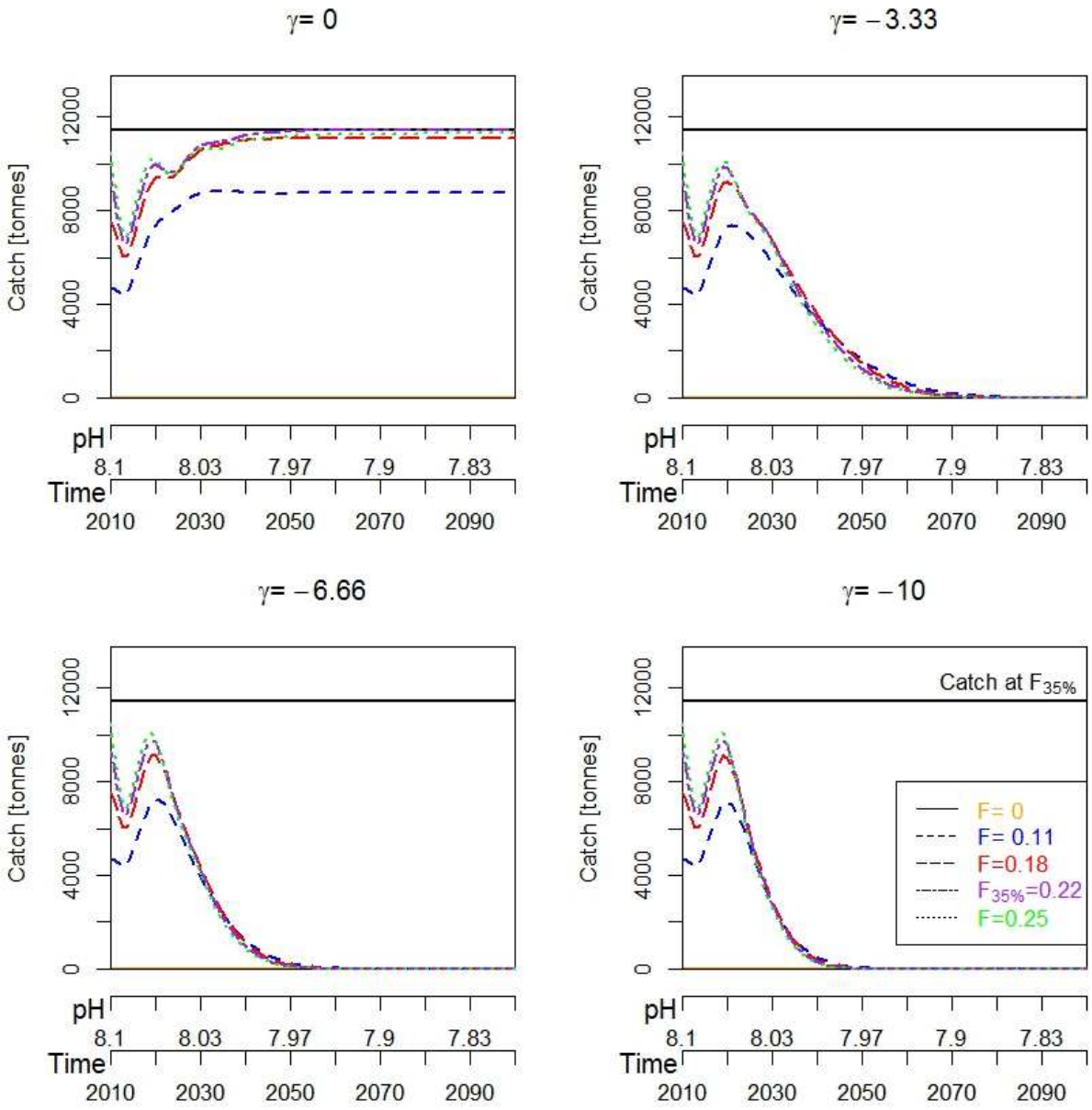

Figure 3.7. Catch of Bristol Bay red king crab under different OA (γ) scenarios for five constant exploitation rates for the directed fishery. The horizontal line denotes the equilibrium catch when the exploitation rate equals $F_{35\%}$ and there is no OA impact.

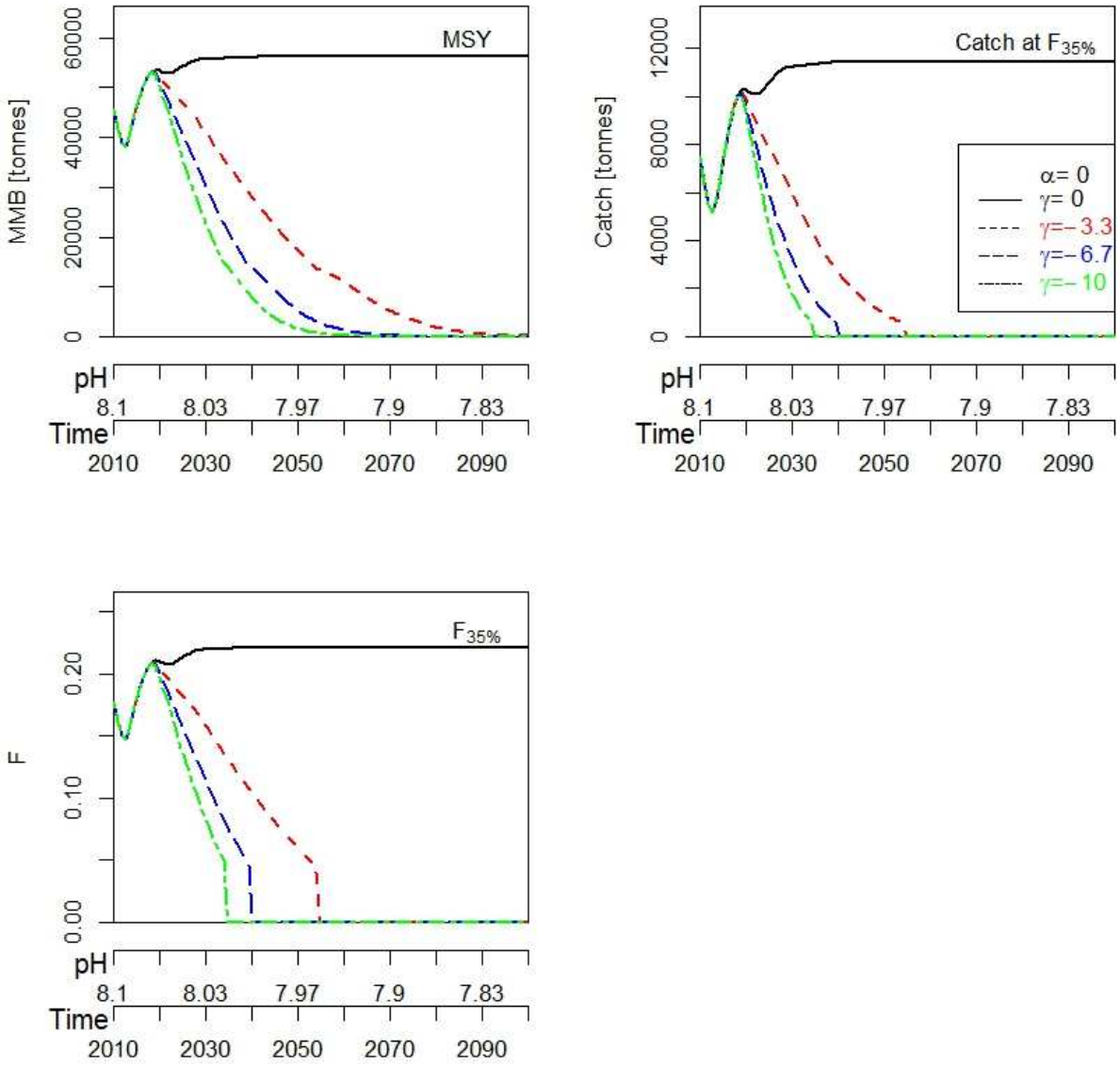

Figure 3.8. Mature male biomass, exploitation rate and catch under different OA (γ) scenarios when the annual exploitation rate is determined using the OFL control rule.

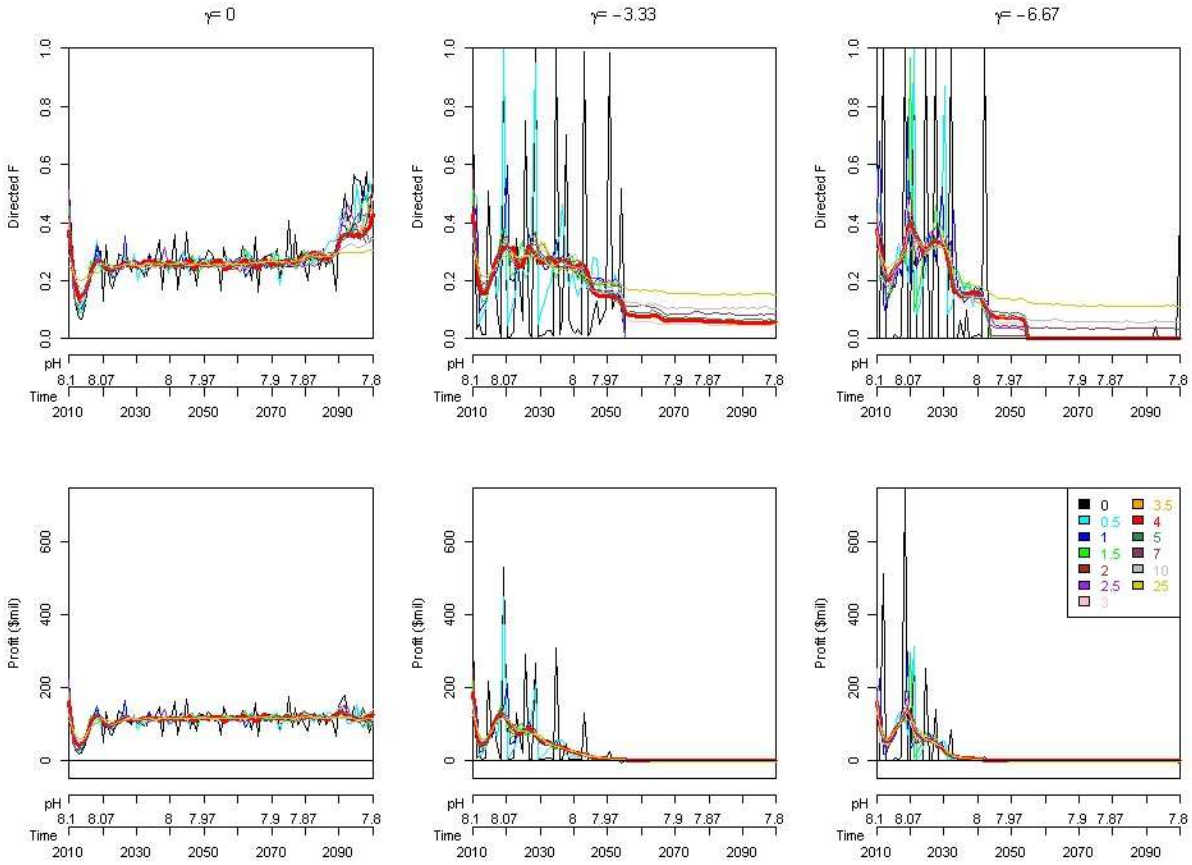

Figure 3.9. Time trajectories of profit and annual exploitation rates when objective function in Equation 3.10b is maximized given a range of values for λ_2 .

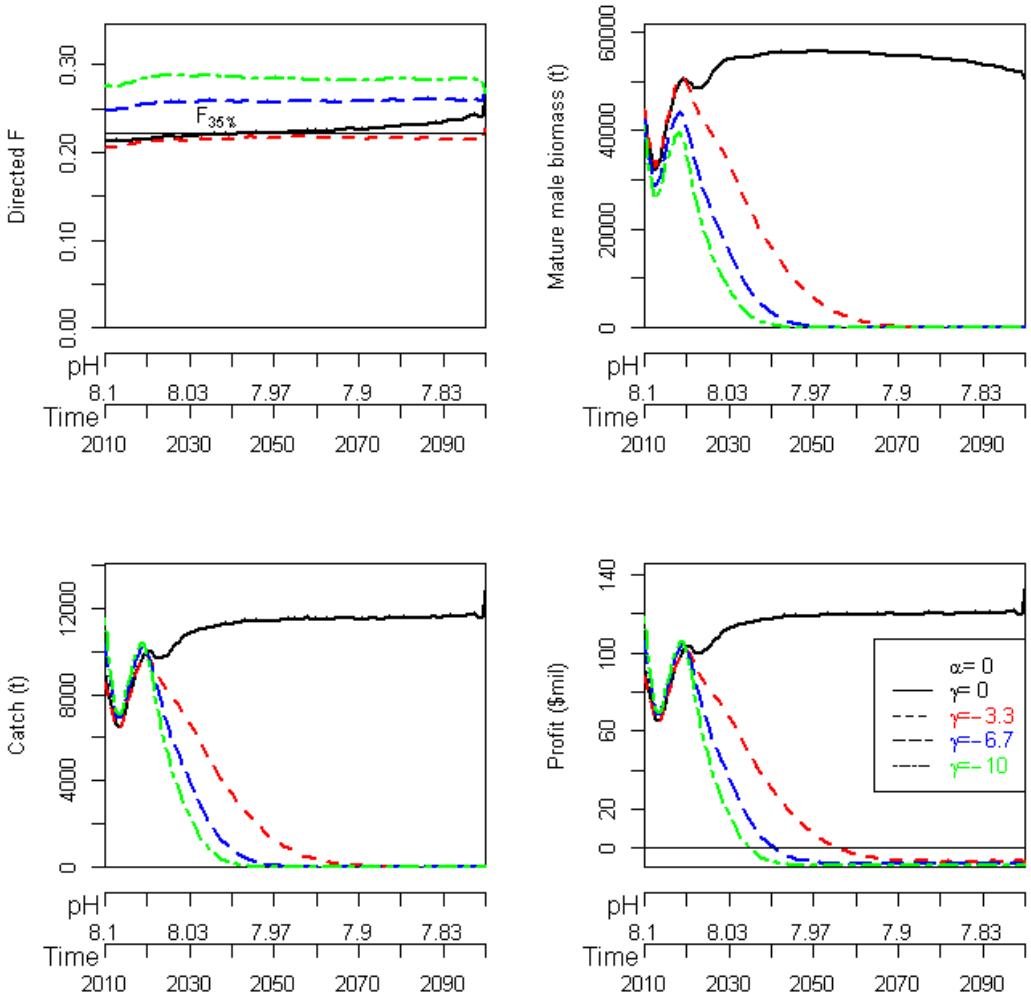

Figure 3.10. Exploitation rate, mature male biomass, catch, and profit under the OA (γ) scenarios when the annual exploitation rate is determined by maximizing catch using the objective function in Equation 3.10a.

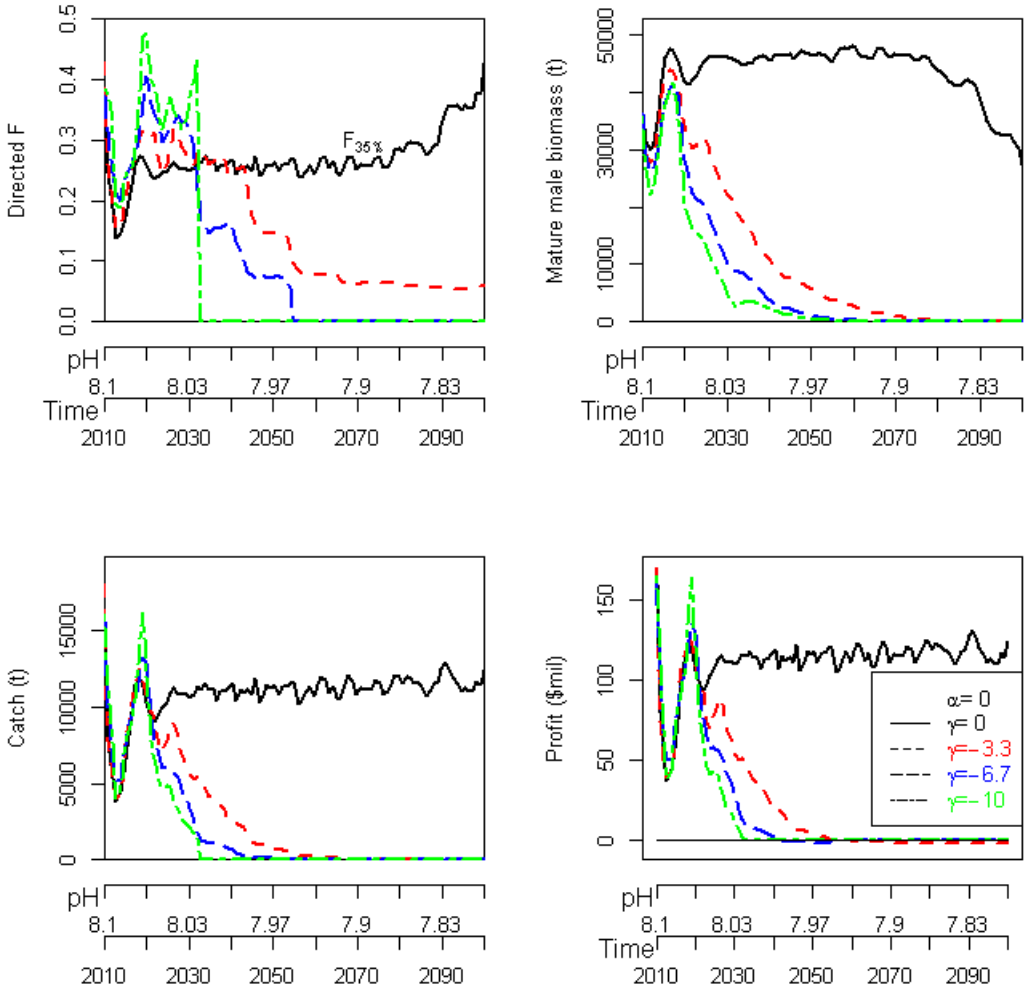

Figure 3.11. Exploitation rate, mature male biomass, catch, and profit under different OA (γ) scenarios when the annual exploitation rate is determined by maximizing discounted profit using the objective function in Equation 3.10b.

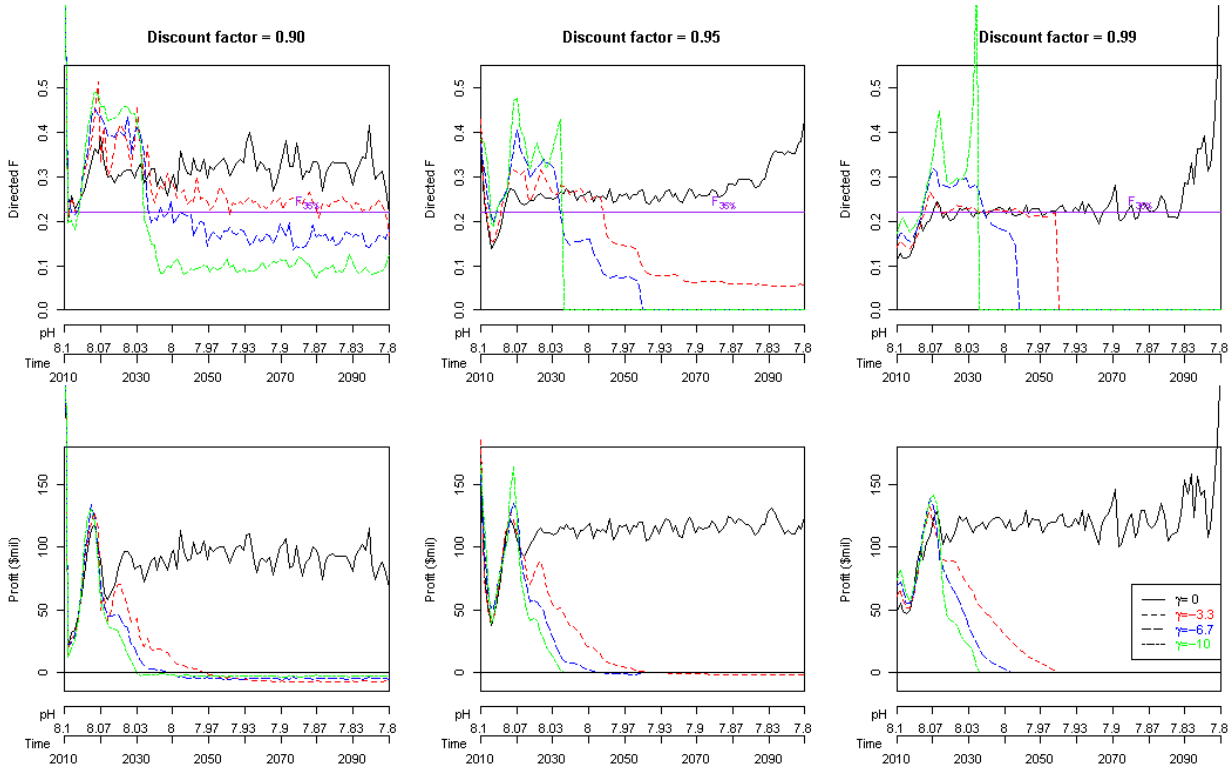

Figure 3.12. Exploitation rates which maximize Equation 3.10b, and the associated time-trajectories of profit for three discount factors (β) and four values of γ .

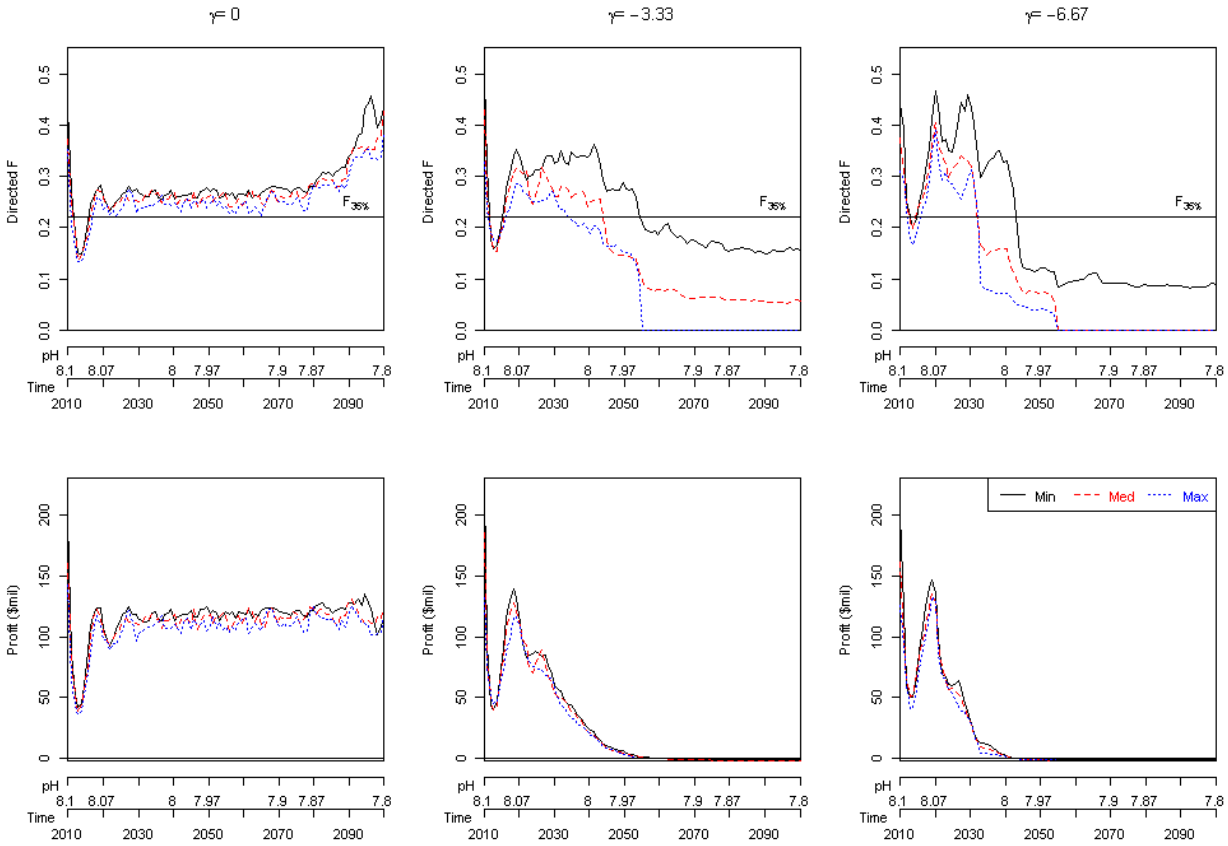

Figure 3.13. Exploitation rates which maximize Equation 3.10b, and the associated time-trajectories of profit for the three cost scenarios and four values of γ.

Figure 3.14 Relationship between the exploitation rates that maximize discounted profit (Equation 3.10b) and MMB for $\lambda_2 = 4$. Initial years (0-10) are omitted.

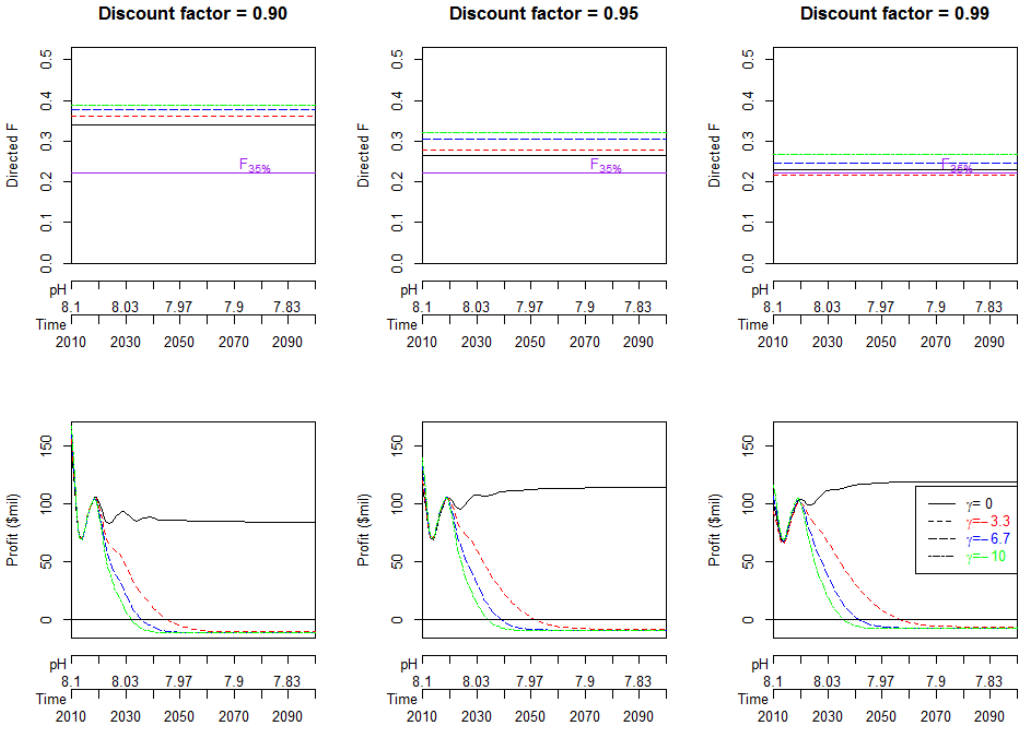

Figure 3.15a. The constant exploitation rates which maximize Equation 3.10c for the three discount factors (β) and all values of γ, and the associated time-trajectories of profit.

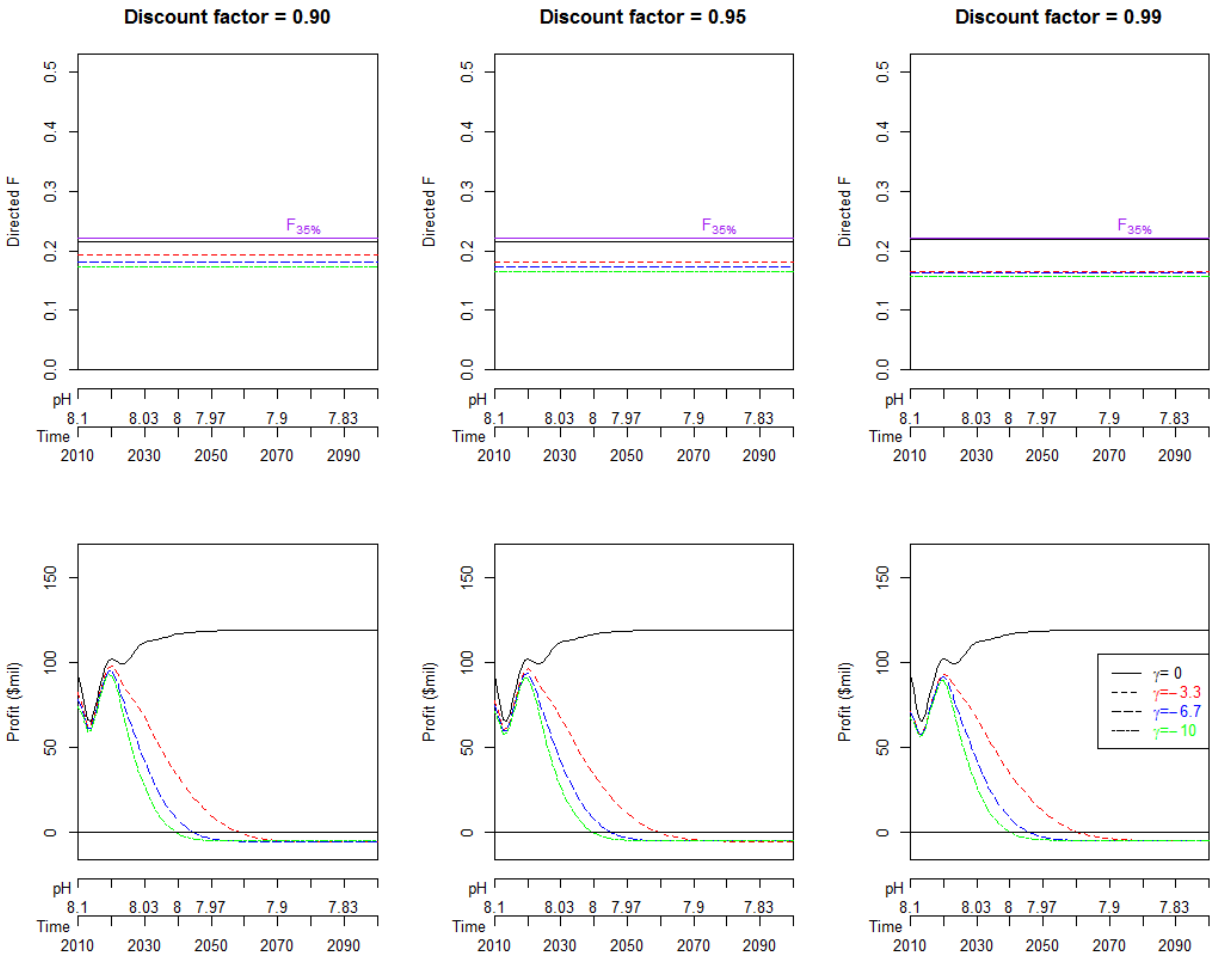

Figure 3.15b. The constant exploitation rates which maximize Equation 3.10c for the three discount factors (β) and all values of γ, and the associated time-trajectories of profit, when the contribution of the first 10 years is omitted from Equation 3.10c.

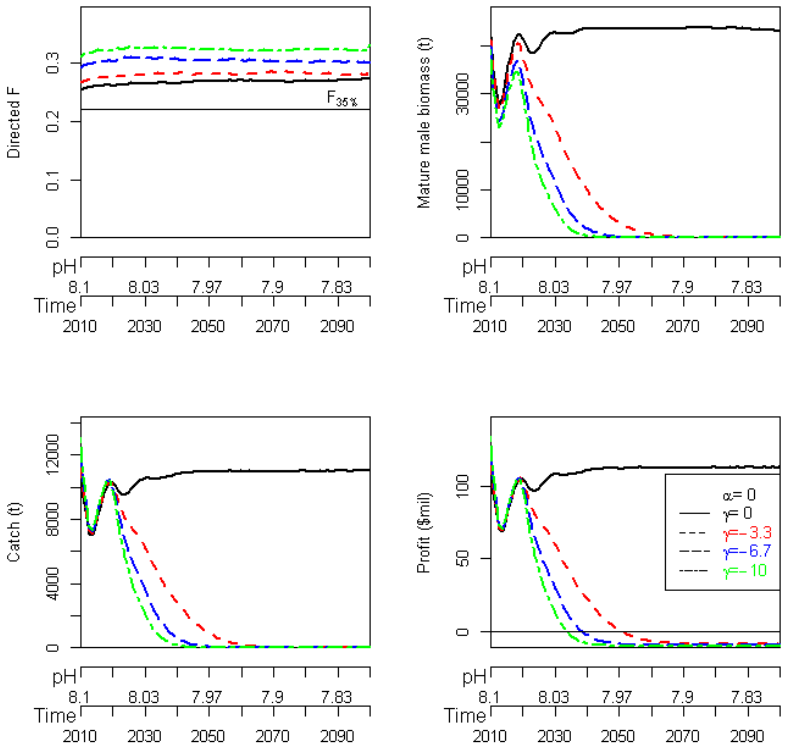

Figure 3.16. Time-trajectories of exploitation rate, MMB, catch, and profit for the four OA (γ) scenarios when the annual exploitation rates are determined by maximizing Equation 3.10c.

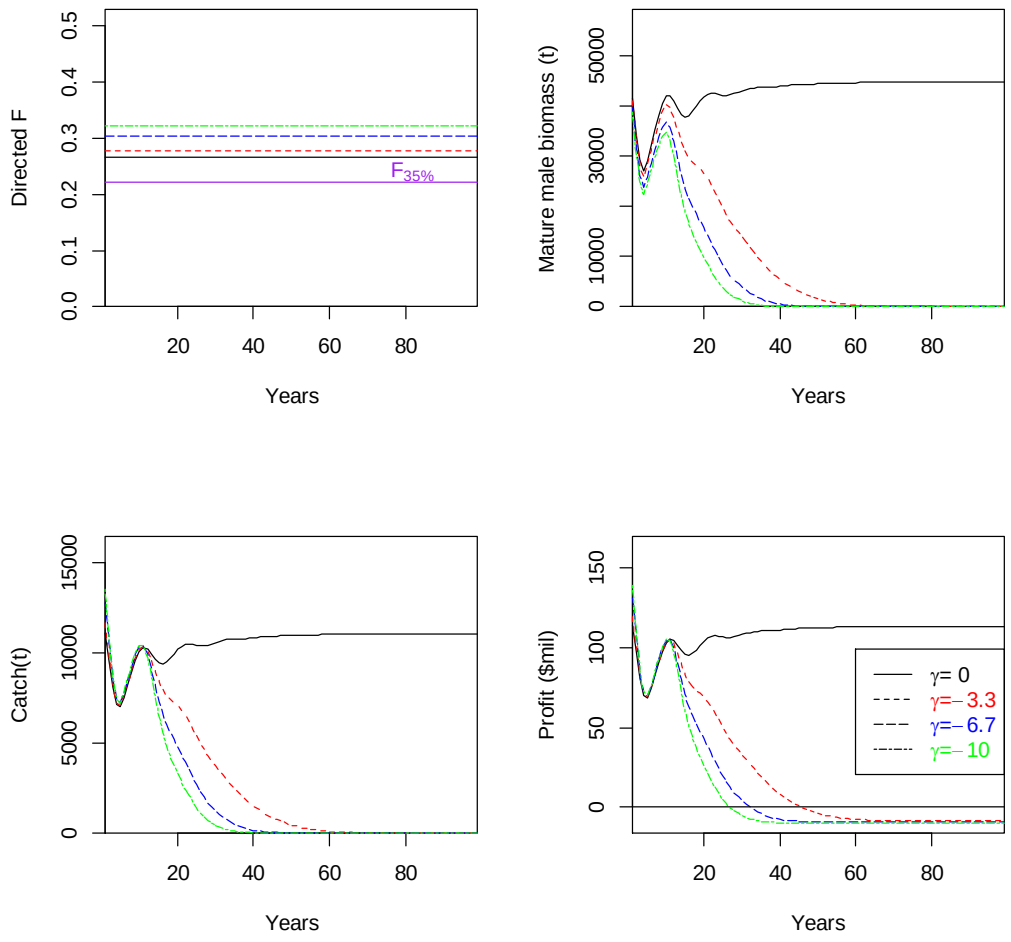

Figure 3.17. Time-trajectories of MMB, catch, and profit for the four OA (γ) scenarios when constant exploitation rates are determined by maximizing Equation 3.10c.

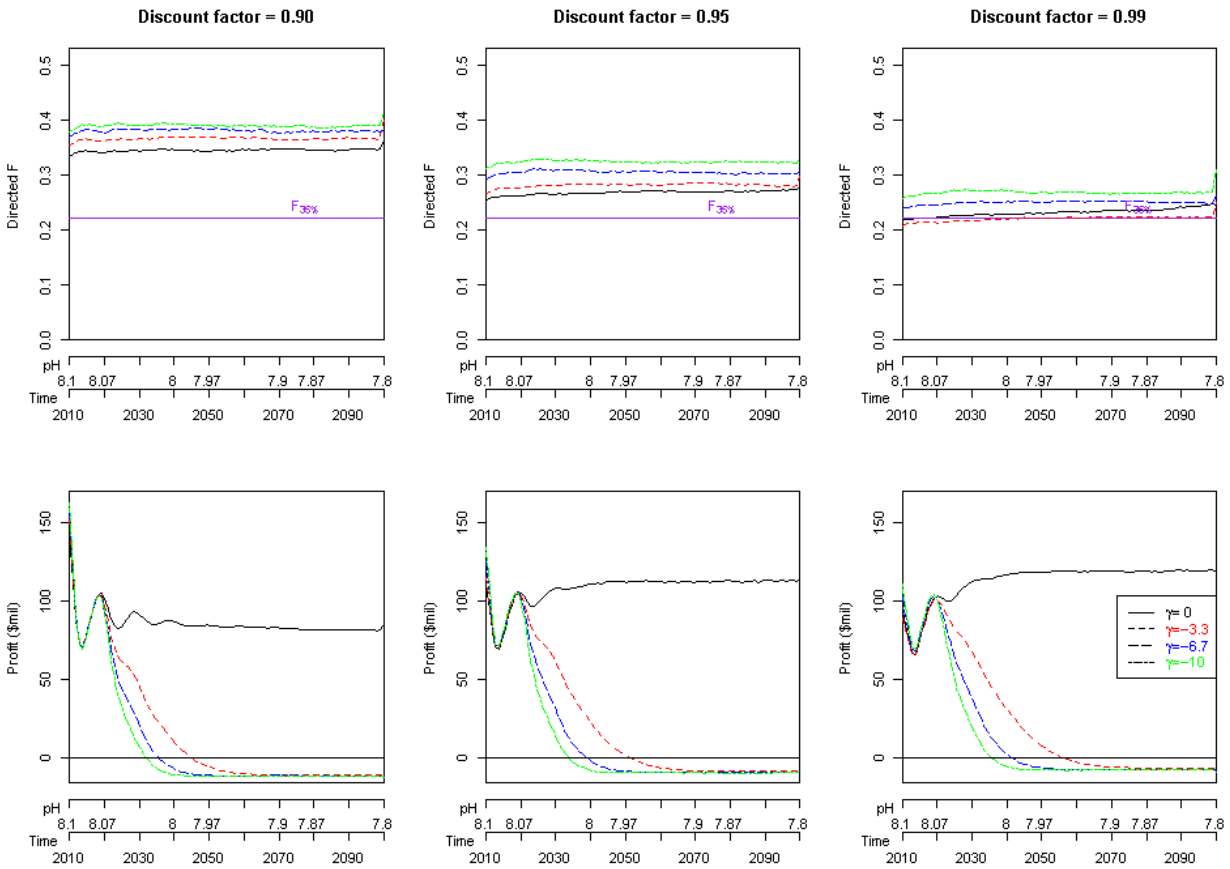

Figure 3.18. Time-trajectories of exploitation rate and profit for the four OA (γ) scenarios when the annual exploitation rates are determined by maximizing Equation 3.10c. Results are shown for three discount factors (β).

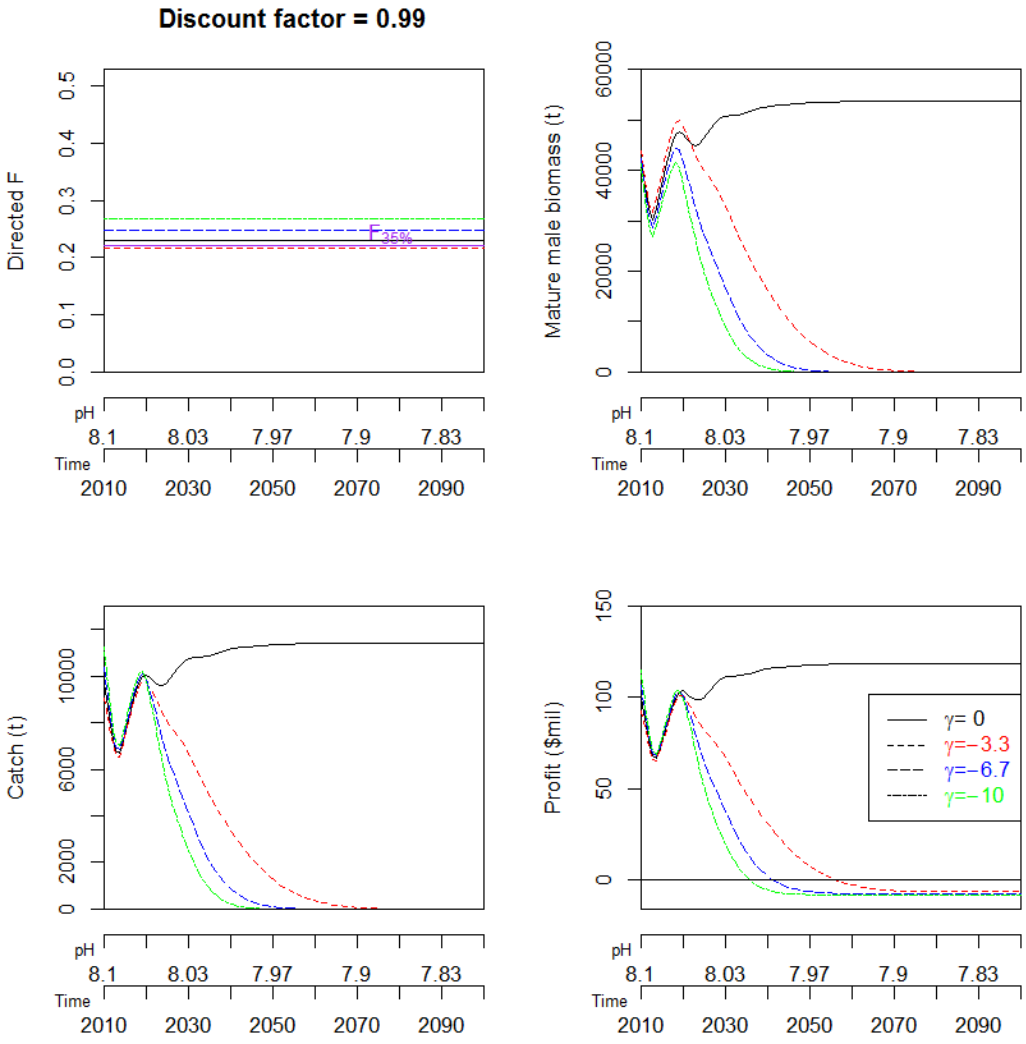

Figure 3.19. Exploitation rate, mature male biomass, catch, and profit for all OA (γ) scenarios when the exploitation rate is determined by maximizing Equation 3.10c given a discount factor (β) of 0.99.

Discussion:

The model developed in this thesis estimates the impact of ocean acidification (OA) on recruitment and yield of Bristol Bay red king crab. It links a model of pre-recruit survival with a simplified version of the model used for stock assessment purposes. The parameters of the pre-recruit model are based on the results from the experiments conducted at the NMFS Kodiak laboratory (Long et al., in press). Specifically, the survival rates under OA in the pre-recruit model cover the range of the survival rates measured during the experiments. The overall survival rate from embryo to the first size-class in the post-recruit model for the (base case) no-OA scenario is set to match the embryo-recruitment survival rate implied by the results of the stock assessment.

The OA impacts on Bristol Bay red king crab and consequently fishery profits depend critically on the pre-recruit survival rates under OA conditions measured during the Kodiak laboratory experiments. However, there are several factors that may have impacted whether the laboratory estimates of survival accurately and precisely represent the survival rates in the open ocean:

(a) the two pH treatments representing conditions in 2100 and 2200 were applied instantaneously, whereas change in pH will be slow in reality, and adaption could take place so survival rates would be higher than predicted from the experiments;
(b) the experiment does not account for any OA impact on the prey species for crab, which would imply that the experimental survival rates may be overestimated;
(c) the Bering Sea is predicted to experience seasonal and regional changes in pH that are more extreme than the modeled pH averages, leading to seasonal patches of pH that would be corrosive to crab shells even by the middle of the 21nd century (Mathis et al., 2011);
(d) the survival estimates are fairly imprecise owing to the fairly small sample size of 30 crab per treatment; and
(e) growth is likely to be impacted by OA, but experiment did not provide information about stage duration times, which if increased would result in lower overall recruitment.

The pre-recruit model predicts the impact of OA on the survival of pre-recruit crab (γ) and their growth rates (α). These two effects are separated in the model so that their impacts can be modeled independently, and compared with observations were they to become available. However, in reality, these two rates are dependent.

Perhaps more important is the impact of OA on adults. The model ignores any impact of OA on growth, which could have consequences for reproductive success if changes in growth impact female migration or molting that now coincide with male migration. The post-recruit model also ignores the impact of OA on the survival rate of post-recruit red king crab, whereas it will likely decrease under OA impacts, consistent with the trend towards lower survival rates under OA for larvae and juveniles as measured during the Kodiak Laboratory research. An decrease in the survival rate for adult red king crab would contribute further to the negative impact of OA on the dynamics of and fishery for, red king crab. The parameters of the Ricker stock-recruitment relationship are assumed not to change under OA. However, it is not clear whether this assumption is valid (NOAA Ocean Acidification Steering Committee, 2010), and it is not unreasonable to expect that the stock-recruitment relationship could become less productive

given unfavorable environmental conditions under OA. Furthermore, a current assumption of the management process and the post-recruit model is that recruitment is a function of MMB. Fertilization rates are therefore ignored and are also not differentiated from the fecundity rates. It is unclear how fertilization rates will change under OA, and whether the number of fertilized eggs will change in proportion to MMB, especially given the extremely low male:female ratio currently estimated by the stock assessment.

Economic parameters such as prices and costs are assumed to be time-invariant, whereas they are likely to change over the next 100 years. The exploitation rates which maximize discounted profit would be higher as would discount profits if prices increased over time, but costs remained constant, and vice versa.

The linked pre- and post-recruit model provides a solid foundation for predicting OA impacts on a crab population if its parameters can be estimated precisely and accurately. However, the link model can improved in several ways such by replacing the linear relationships between survival and growth and pH by relationships which fit the experimental data better, and by allowing for impacts of OA on survival and growth of post-recruit crab.

Bristol Bay Red king crab fishery is one of the 10 king and Tanner Crab fisheries in the Bering Sea and Aleutean Islands which are under joint Federal-State management. Each of the 10 stocks is assigned to a management tier (1-5), which defines how management rules are applied. Bristol Bay red king crab, and EBS Snow and Tanner crabs are tier 3 stocks for which reliable estimates of the stock-recruitment relationship are not available, but proxies for F_{MSY} and B_{MSY} can be estimated based on the assumption that $F_{\mathrm{MSY}} \sim F_{35\%}$. Tiers 1 and 2 (currently, no stocks) have more reliable information on F_{MSY} and B_{MSY} than tier 3 stocks, and tier 4 (Pribilof Islands blue king crab (overfished 2011/12), St. Matthew blue, Pribilof Island red, and Norton Sound red king crabs) and tier 5 (Aleutian Islands golden, Pribilof Islands golden, and Adak red king crabs) stocks have insufficient information to estimate the stock-recruitment relationship or estimate $F_{35\%}$.

This model can be modified to predict OA impact on the other tier 3 stocks, because the stock-recruitment relationships for those stocks can be parameterized under the assumption $F_{\mathrm{MSY}} \sim F_{35\%}$. There is currently no obvious way to parameterize stock-recruitment relationships for stocks in tiers 4 and 5, and so this approach outlined in this thesis cannot be directly applied to them. However, an inference regarding the impact of OA on these stocks can be made given predicted catches under OA for the tier 3 stocks, as the stocks in tiers 4 and 5 have been managed using a GHL based on long-term average harvest. This inference will become more meaningful as the data describing OA impacts on tier 4 and 5 stocks becomes available from the Kodiak Laboratory.

The Kodiak Laboratory is currently conducting further experiments related to OA impacts on red king crab, Tanner crab, and golden king crab. These experiments involve not only pH treatments, but also treatments involving changes in temperature, which makes the experiments more realistic and provide further data for use in parameterizing pre-recruit models. The results of the additional experiments are planned to become available in Fall 2013. Further research on embryonic, larval, and juvenile crab, which are considered the stages most likely to be vulnerable to OA, has been proposed for red, blue, and golden king and Tanner crab stocks.

Immediate issues for management of the tier 3 crab stocks under OA related to MSST and recruitment:

i. MSST is currently defined as ½ of B_{MSY} for Alaskan crab stocks, but there is no definition for B_{MSY} for stocks impacted by ocean acidification.

ii. The assumption that recruitment is related to MMB may be invalid, in particular because the decrease in fertilization rates under OA might not be proportional to the decrease of MMB.

References:

Long W.C., Swiney, K.M., Harris, C., Page, H.N., and Foy, R.J. *In press*. Effects of ocean acidification on juvenile red king crab (*Paralithodes camtschaticus*) and Tanner crab (*Chionoecetes bairdi*). Kodiak Laboratory, Resource Assessment and Conservation Engineering Division, Alaska. FSC, NMFS, NOAA.

Mathis J.T., Cross J.N., and Bates N.R. 2011. The role of ocean acidification in systemic carbonate mineral suppression in the Bering Sea. Geophys. Res. Lett. 38: L19602.

NOAA Ocean Acidification Steering Committee. 2010. NOAA Ocean and Great Lakes Acidification Research Plan, NOAA Special Report, 143 pp.

Zheng, J., and Siddeek, M.S.M. 2010. Bristol Bay red king crab stock assessment in fall 2010. In: 2010. Stock Assessment and Fishery Evaluation Report for the King and Tanner Crab Fisheries of the Bering Sea and Aleutian Islands Region: 2010 Crab SAFE. North Pacific Fishery Management Council, Anchorage.